1-1-2020

# Comparing The Variability Of Natural Sand To The Variability Of Sand Containing A Simulant Land Mine

Anna Marie McWhirter

Follow this and additional works at: https://egrove.olemiss.edu/etd

COMPARING THE VARIABILITY OF NATURAL SAND TO

THE VARIABILITY OF SAND CONTAINING A SIMULANT LAND MINE

A Thesis

Presented for the

Master of Science

Degree

The University of Mississippi

Anna Marie McWhirter

May 2020

ABSTRACT

Understanding the relationship between excitation sources, buried target (i.e., buried hazard, land mine, acoustic article) response, and soil properties is fundamental to improve laser-ground-vibration sensing methods. This project investigates the natural soil's behavior under acoustic stimuli and compares soil behavior with a buried target through geostatistical methods. Vibrational velocity of sand is measured with an LDV in a confined box filled with and without a buried target. Geostatistical calculations were performed on standardized data (e.g., background velocity and with-target velocity) sets to observe spatial variability. The standardized background velocity is mean 0 and variance of 1, while the addition of the target increases the variance to 27X the background. The background variability resembled uncorrelated white noise. The with-target variogram reveals structural features indicative of the target size and location in the measurement grid. Sensitivity studies evaluate the impact of fewer data and uncorrelated, correlated, and trending noise in the off-target soils. In a subdomain of the measurement grid, the structure of the target is preserved in the variogram and correlate with the size of the grid and surrounding encounters with off-target points. Systematically removing velocity points preserved the target presence with slight changes in the variogram structure according to new separation distances. When uncorrelated noise replaced off-target observations, the target is interpretable from the variogram up to a variance of over 400. Alternatively, when a random field with fixed correlation lengths is applied, the target is obscured at higher variances. Trended data added to off-target

observations attempts to simulate field parameters. At increasing variances, strong trends in the background obscure the target. Geostatistical characteristics revealed through data sensitivity studies provides a robust indicator of target presence up to applications of high variability. Small-scale variation in sand provides features indicative of target presence. This study suggests that understanding the spatial structure of the acoustic response of natural soils is critical to the development of land mine detection technologies using an LDV. Future studies should focus on collecting experimental data from field sites.

DEDICATION

I dedicate this work to my mother, Barbara McWhirter. She remains my biggest cheerleader to this day, and I am forever grateful for her enthusiasm and support in my life achievements. I would also like to dedicate this to the loved ones lost, for they are a light shining down on me always.

## LIST OF ABBREVIATIONS OR SYMBOLS

NCPA – National Center for Physical Acoustics

LDV – Laser-Doppler Vibrometer

HVSR – Horizontal to Vertical Spectral Ratio

A/S – Acoustic-to-Seismic coupling

FM – Frequency Modulated

FFT – Fast Fourier Transform

PRN – Pseudo-Random Noise

MAD – Median Absolute Deviation

Z – Standardized Variable (Z-score)

$\sigma$ – Standard Deviation

$\mu$ – Mean

h – Separation Distance

C(h) – Covariance as a function of separation distance

$\gamma$(h) – Variogram Value as a function of separation distance

RF – Random Field

$\sigma^2$ – Variance

## ACKNOWLEDGEMENTS

"see you later." Thank you to previous graduate students who still keep in touch and gave me advice or encouragement when you knew I needed it.

Lastly, thank you to my mother, my best friend, my rock. You have supported my dreams from day one and I am blessed God gave me you.

TABLE OF CONTENTS

LIST OF TABLES

LIST OF FIGURES

# I. INTRODUCTION

The investigation of excitation sources, buried target (i.e., buried hazard, land mine, acoustic article) response, and soil properties is fundamental to improve laser-ground-vibration sensing methods. Utilizing a non-contact detection system to examine vibrational soil response in different environments/media will reflect the behavior of the soil under acoustic stimuli. In order to understand the soil's variability when a buried target is present, the study must include a control – soil without a buried target. Modeling the natural background variations in soil is significant in detecting land mines because it provides contrasting properties when compared to soil containing a land mine (Donskoy, et al., 2002; Scott, et al., 2001). The characterization of the natural background variability of different types of soil provides information about near-surface behavior. Geostatistical approaches can quantify the spatial variability of ground surface response to acoustic and seismic excitation.

The acoustic-to-seismic coupling-based detection technique that utilizes a laser Doppler vibrometer (LDV) has been applied to obtain soil vibration response (Arnott and Sabatier, 1990; Sabatier and Xiang, 2001; Xiang and Sabatier, 2003, 2004). Using technology such as a laser Doppler vibrometry to measure soil vibrations is a less invasive method than using geophones (Harrop and Attenborough, 2002). A geostatistical comparison of the soil's response with and without a buried target will aid in the detection process of actual land mines that have caused problems and continue to be prevalent in parts of the world affected by war.

The purpose of this project is to investigate the natural soil's behavior under acoustic stimuli and make a comparison to soil behavior with a buried target through geostatistical methods. Vibrational velocity of sand is measured with an LDV in a confined box filled with and without a buried target. In data conditioning, the velocity observations were investigated for outlier peaks and edge effects, which ultimately reduce the measurement grid. Standardizing the velocity sets after completing data conditioning better compares the distribution of values. Geostatistical calculations were performed on the final data (e.g., background velocity and with-target velocity) sets to observe spatial variability. The with-target variability characteristics were evaluated by conducting sensitivity studies to assess the impact of directionality, reducing the number of points observed, adding noise, correlation, and trends to off-target data.

The standardized background velocity is mean 0 and variance of 1, while the addition of the target increases the variance to 27X the background. The with-target variogram reveals structural features indicative of the target location in the measurement grid. An arbitrary frame positioned on the center of the with-target data moves to position the target in the corners. The structure of the target is preserved in the variogram and correlate with the size of the grid and surrounding encounters with off-target points. Data decimation examines the variability at greater spatial differences. Systematically removing velocity points preserves the target presence with slight changes in the variogram structure according to new separation distances.

Noise generated at different variances replaced off-target observations. The target signature in the variogram is preserved until high variances. Noise with fixed correlation lengths affects the variograms in a similar manner, but becomes nonergodic at high variances and masks the target influence on variability. Trended data added to off-target observations attempts to simulate field parameters. At increasing variances, the trends create a correlation length in the

2

variogram beyond the size and location of the target. Geostatistical characteristics revealed through data sensitivity studies provides a robust indicator of target presence up to applications of high variability. Small-scale variation in sand provides features indicative of target presence.

## II. BACKGROUND

GEOSTATISTICS

Geostatistical approaches have been used to characterize natural phenomena since the 1950's when Krige (1951) noticed that classic statistical methods paid little attention to the analysis of geologic problems. Common statistics do not consider the spatial aspect of the studied distributions (Matheron, 1963). As a result, geostatistics is useful for studying the spatial and temporal distributions of such properties, as salinity, moisture content, and permeability. Matheron (1963) was one of the first to apply geostatistical functions, known as regionalized variables, having a number of qualitative characteristics: 1) the regionalized variable is localized, where its variations occur in space; 2) the variable may have varying degrees of continuity in its spatial variation through deviation between the same properties of neighboring samples; 3) the variable may exhibit anisotropies, where properties may vary greatly along a certain direction or cross-direction. These three spatial characteristics of the regionalized variables are the foundation of geostatistical methods. In general, a regionalized variable is a synonym for a stochastic process, random process, or random field (Matheron, 1963).

The regionalized variable was introduced into soil science in the 1980's and used as an approach for the spatial estimation of soil properties (e.g., Brus and Gruijter, 1997). Numerous papers concluded that classical statistics were not suitable for Earth sciences because they assumed that data were independent (Burgess and Webster, 1980; Burgess et al., 1981; Oliver et

4

al., 1989; Webster, 1985). In terms of site characterization data, random variables are not distributed identically or independently (Barnes, 1988). There are many factors that affect the spatial distribution of soil properties such as moisture content, vegetation, and stratigraphic heterogeneity. Soil variability is the result of these properties working together across a range of scales to exhibit a certain behavior. Furthermore, soil variability manifests as variability in the results of acoustic or seismic response of soil. The quantification of soil variability from acoustic and seismic measurements are not well developed. The horizontal to vertical spectral ratio (HVSR) technique assume a random distribution of subsurface seismic sources which can be related to subsurface variability.

Geostatistics is a frequently used method to characterize the variability of soil response in space, with the variogram as a classic mathematical tool (Matheron, 1963). The variogram illustrates the variation of a property of interest in a sample set as distance increases between samples. Matheron (1963) describes it as the influence zone of a sample set and that the characteristics of the regionalized variable are well represented by the variogram. A few important features expressed in the variogram include: range, sill, and nugget effect (Isaaks and Srivastava, 1989). The spacing between paired samples is the separation distance. The variogram value is half the average squared difference between paired data values. Increasing separation distance between pairs generally causes the variogram to increase as well. When the increase in separation distance no longer affects the variogram value, the variogram reaches a plateau. The range is the value of separation distance to this plateau. The sill is the variogram value where the range begins. When the separation distance is zero, the variogram value is zero. When the variogram achieves the sill value at the smallest separation, it is a nugget variogram, which can be caused by several factors, including: sampling error and short scale variability. At very small

separation distances, sample values that are fairly different can cause a discontinuity at the origin of the variogram. The nugget effect is the apparent value of the variogram at zero separation distance (Isaaks and Srivastava, 1989).

An omnidirectional variogram is useful, but it neglects the direction that the separation distance vector propagates; however, the omnidirectional variogram is simply a helpful starting point and does not suggest that the spatial distribution is the same in all directions (Isaaks and Srivastava, 1989). An omnidirectional variogram with erratic behavior could indicate an underlying problem in the data set. It can also be an indicator of a directional variogram, where anisotropy is a descriptive pattern of directional variogram behavior.

Another important geostatistical tool is the auto-covariance function, and it also represents how spatial continuity changes as a function of distance and direction (Isaaks and Srivastava, 1989). When two random variables are close together, it would be expected that they share similar properties and have a large covariance (correlation). It is merely the standard covariance function between two random variables. Consequently, the covariance of a random variable and itself is the same as the variance. When a random field is correlated in space, the auto-covariance function will decrease as the distance between two points decrease. Successively, the correlation length will move toward zero past a certain distance, and random variables appear uncorrelated at distances beyond the correlation length. The auto-covariance function is a useful spatial statistic for providing insight to the strength of correlation in the system.

Literature about spatial variability of soil properties using geostatistical approaches is extensive; however, the current study examines the spatial distribution of soil vibration at sensor-measured points, where there is a lack in literature available on this topic specifically. The

vibrational response of soil is induced by an excitation source and the displacement of soil particles is measured by a sensor. Subsequently, geostatistical approaches were taken to quantify soil response. Quantification of this behavior is significant for the detection of buried hazards, also referred to as buried targets, land mines, and acoustic articles. The purpose is to be able to differentiate the natural variability of the soil from the variability of the soil containing a buried hazard.

## MEASURING ACOUSTIC-TO-SEISMIC COUPLING WITH AN LDV

Lamb (1904) observed the coupling of airborne sound into the earth, but further examination was conducted through a series of studies in the 1950's (Press and Ewing, 1951a; Press and Ewing, 1951b; Jardetzky and Press, 1952; Press and Oliver, 1955; Biot, 1956; Bass et al., 1980). Well-documented in the literature, acoustic energy striking the ground surface producing seismic motion is a phenomenon known as acoustic-to-seismic coupling (A/S) (Bass et al., 1980; Hickey and Sabatier, 1997; Sabatier et al., 1986a; Sabatier et al., 1986b; Sabatier and Xiang, 2001). Starting around the 1980's, numerous experimental studies have characterized the seismic surface velocity and acoustic sound pressure response in poroelastic media from an excitation source, such as an acoustical or mechanical source (e.g., Sabatier et al., 1986a; Sabatier et al., 1986b; Hickey and Sabatier, 1997). Air-filled porous soil exists in the shallow region below the ground surface and allows seismic motion to couple to the skeletal frame of the soil through momentum transfer and viscous drag at the porous walls (Sabatier et al., 1986a; Sabatier et al., 1986b; Xiang and Sabatier, 2003). The seismic motion below the surface induces vibration at the ground surface due to A/S and is detectable by noncontact techniques, such as an LDV (Arnott and Sabatier, 1990; Harrop and Attenborough, 2002).

The LDV emits a laser beam onto a vibrating surface, measuring points on an area of interest. The vibrating surface particles cause a Doppler frequency shift of the reflected light from the beam on the surface. The backscattered light travels back to the LDV and is measured by a photo-detector. A frequency-modulated (FM) signal from the photo-detector carries the surface velocity information (Sabatier and Xiang, 2001; Xiang and Sabatier, 2003). Additional details about the LDV can be found in Scruby and Drain (1990). The LDV is useful to the detection of buried hazards, for they are usually buried at shallow depths (Xiang and Sabatier, 2003). The motion of the ground surface is noticeably different when a buried hazard is present. Resonating buried hazards cause the surface to vibrate with greater amplitude and can be detected by measuring surface vibrations (Muir et al., 2014). The acoustical compliance of the buried hazard is different from the surrounding soil, so the dynamic interaction of the buried hazard with the surrounding soil will exhibit linear and nonlinear effects different than the natural soil (Donskoy et al., 2002). The LDV has been used for land mine detection in numerous studies, (e.g., Donskoy et al. (2002); Korman and Sabatier (2004); Xiang and Sabatier (2004); Muir et al. (2014)) and the LDV began to demonstrate promising results for land mine detection in the 2000's according to Aranchuk and Sabatier (2006).

With successful laboratory experiments using the LDV for land mine detection, additional studies, such as the current study, will help to understand the impact of spatial variability in the soil surrounding land mines on land mine detection. Geostatistical approaches characterize the soil vibration response that the natural soil exhibits from one location to another. Since the surrounding soil vibrates differently when a buried hazard is present, the use of an LDV provides a noninvasive method in determining the spatial distribution of soil vibration

(Harrop and Attenborough, 2002). A geostatistical analysis of surface vibration can reveal spatial relationships displayed by the soil and the influences of a buried hazard.

## III. METHODS

### MEASUREMENT SYSTEM

A Polytec Scanning Vibrometer PSV 300 system measured sand vibration and controlled the acoustic excitation source. The individual components included: Vibrometer Scanning Head-056, Controller OFV-3001 S, Junction Box PSV-Z-040, and Workstation PSV-PC. The Vibrometer Scanning Head was mounted on a fully extended tripod in front of a wooden sandbox with dimensions of 97 cm by 146 cm and 45 cm deep (Figure 1A). The sound source used to excite the sand was a Peavy Impulse 200 speaker system suspended roughly 1 m above the sandbox surface (Figure 1A). There was no contact between the tripod or wooden box with the loud speaker to avoid direct mechanical vibration transfer. Polytec Scanning Vibrometer PSV 300 system provided its own data processing, acquisition, and visualization. The controller moves the beam from the LDV head around the specified grid with a two-axis mirror. It also produces the source low-level acoustic signal for the speaker. This signal is further amplified by an Electro-Voice P3000 amplifier to power the speaker to achieve the desired amplitude. The output from the controller of the Polytec system are complex Fast Fourier Transform (FFT) data that included complex velocity vectors at each point as a function of the corresponding frequency vectors.

EXPERIMENTAL DESIGN

Playground sand bought from Home Depot was placed in a sandbox. The surface was smoothed and a developer was sprayed on the surface to create a white mist layer to help the laser beam reflection. Initially, a control measurement of the sandbox without a buried target was obtained. Then, an empty plastic tub with a bottom diameter of 16.2 cm, a lid diameter of 18.1 cm, and a height of 6.7 cm (Figure 1B) was placed upside down at a depth 0.76 cm.

GEOPHYSICAL METHODS

The LDV scanned a predefined grid of 31 rows and 37 columns, with 1147 points (Figure 2) with a two-axis mirror. The excitation signal consisted of either pseudorandom noise (PRN) or swept sine with a frequency band of 40 – 140 Hz. Experimental results from Xiang and Sabatier (2003) found that the optimal frequency range for antipersonnel (AP) mine detection was between 100 and 680 Hz. The Polytec software recorded and processed the frequencies between 40 Hz and 400 Hz. After a successful acquisition of the control or background measurement (i.e. without a buried target) using PRN, the plastic tub was placed in the sand. With the buried target, the speaker system emitted 95 dB using a sweep of 40 – 400 Hz in steps of 4 Hz. This band of 40 – 400 Hz captured the resonating frequency of the buried target. During both trials, the laser beam measured the instantaneous vibrational velocity response of the sand as a function of frequency at each point of the grid.

DATA PROCESSING, ACQUISITION, AND VISUALIZATION

A Matlab code was developed to geostatistically analyze the spatial variation of the instantaneous vibrational velocity at all frequencies. The LDV data from the sand without a buried target was used to characterize the natural background variability. The natural variability from the control results were then compared to the results with a buried target. The magnitude of the complex vectors produced velocity in units of meters per second. All of the velocities at each point on the spatial grid at a given frequency were assigned separate vectors in one matrix, so the matrix is reshaped into a 31 by 37 grid with 1,147 observations. This results in 91 dimensions of 31 by 37 matrices. The dimensions start at 40 Hz and step by 4 Hz to 400 Hz.

DATA CONDITIONING

Comparing the spectrograms of the measured surface velocity of a point above the buried target to a point off the target or a point without the target (Figure 3) indicates a primary target resonance at 64 Hz and a secondary resonance at 128Hz. Velocity maps, at 64 Hz, of the background velocity (Figure 4A) and with a target present (Figure 4B) have very different ranges.

The velocity map with the buried target (Figure 4B) demonstrates the vibrational effects of the buried target near the center of the box but also contains velocity measurement irregularities (i.e., data spikes) possibly due to a bad LDV signal produced from speckle patterns. The target signature is masked by these outlier spikes. Furthermore, there were larger velocities near the edges of both data sets suggesting edge effects from the wooden box holding the sand.

Stacked histograms of the velocity measurements (at 64Hz) with and without a buried target are displayed in Figure 5. The points in off-target locations and the data without a target

are distributed at low velocity. The data on top of the target and outlier spikes are expressed on the tail end of the histogram, creating an odd distribution. The means and variances of the entire data sets are presented in Table 1. The off-target points were referenced in the table determined by removing velocity values in the target location that were at least twice as large as its nearest neighbors.

The mean of the off-target data and the background (controlled or without target) are similar (Table 1). The larger off-target data variance is associated with outlier spikes in the data and possible choice of the off-target domain. Data including the target has larger mean and variance due to the localized large velocity above the target.

An outlier detection and replacement code was developed to mitigate outlier points in both the background velocity and velocity with a buried target by classifying outliers as values more than three scaled Median Absolute Deviation (MAD) from the median.

$$MAD = c * median(|V_i - median(V)|), \quad where \; c = -\frac{1}{\sqrt{2} * erfcinv\left(\frac{3}{2}\right)} = 1.4826 \quad (1)$$

Figure 6 and 7 display the measured velocity values (blue lines) and the upper velocity threshold (yellow horizontal line). Values greater than the threshold were replaced with the value of the upper threshold. The velocity values after outlier replacement are denoted by the open circles. The means and variances after replacement are presented in Table 2. The off-target points were most influenced by outlier replacement. The variance decreased by two orders of magnitude, but the mean did not have a significant change. The background and with-target points did not change by a substantial amount.

The influence of the wooden container edges and reduction of the measurement grid was determined using the means and variograms of strips of data across the x- and y-directions. The goal was to effectively remove data points where the ratios of the strips to the entire grid that

were greater than 1.15. Due to irregular sample spacing, the grid strips in columns and rows were analyzed separately to provided boundaries for reduction of the measurement grid. The original grid for both data sets (with and without target) had 31 rows and 37 columns with 1,147 observations. Four strips of five rows were selected starting at the edge of the measurement domain and moving inwards but being careful to avoid the influence of target resonance. Figure 8 shows the selection of strip rows for the background (without target) data and Figure 9 shows the selection for the target data. The selection of column strips is grouped in a similar fashion and shown in Figure 10 and 11, respectively.

## GEOSTATISTICAL METHODS

Grid points labeled with variables $i$ and $j$ each represented point 1 to N scalar observations to indicate the row and column grid positions $(x_i, y_i)$ and $(x_j, y_j)$. A matrix of separation distances was created from the grid positions used as sample locations. Indexing deleted repeating points in the bottom half of the matrix of separation distances. The number of pairs between points was found and did not include duplication of pairs or zero separation distance between pairs.

The covariance and variogram matrices were calculated using a modified version the following equations from Isaaks and Srivastava (1989),

$$C(h) = \frac{1}{N(h)} \sum_{(i,j)h_{ij} \approx h} v_i \cdot v_j - m_{-h} \cdot m_{+h} \tag{2}$$

$$\gamma(h) = \frac{1}{2N(h)} \sum_{(i,j)h_{ij} \approx h} \left( v_i - v_j \right)^2 \tag{3}$$

where, $v_{i,j}$ = data values, $m_{\mp h}$ = mean of all data values, $h$ = separation distance, $N$ = number of pairs. Indexing deleted repeated points in these matrices as well. The matrices of covariance and variogram values were reordered into a vector by the value of corresponding separation distance. A summation scheme used the covariance values, number of lags, and lag range to calculate the values used to create covariance plots and variograms. After covariance was calculated, it was decided not to be used because it is the inverse of the variogram and would not provide additional characteristics relevant to the objective. This scheme created omni-directional variograms for group sample pairs that share similar spacing (Isaaks and Srivastava, 1989). The Matlab code is applied to both the data from the test with and without a buried target. Additional code was used to visualize the vibrational velocity on different frames of the reduced grid and at other resonating frequencies. These visualizations allowed for better understanding of the vibrational response from acoustic excitation. The Matlab code is provided in Appendix A.

Variograms of the background and off target points when moving from the top row (Figure 12A) or bottom row (Figure 12C) towards the center of the grid (Figure 12B and 12D), become closer to one another, which implies that the velocity values are distributed more equivalently. In the columns, the variograms for each data set move way from one another, even though it is at a small scale. Although, the variances continually decrease when moving inwards from columns 1 to 5 and 33 to 37 to columns 6 to 10 and 28 to 32, respectively. The mean and variance as well as the ratios of the strip value to the entire grid are tabulated in Table 3 for the rows and Table 4 for the columns. The mean and variance of the top row in the off-target data is substantially larger than the background data and larger than the entire grid values. Other rows are very similar and close to the behavior of the entire grid (ratios > 1). This suggests that there is some influence of the top boundary of the box. The column strip data (Table 4) along the right-

side edge has a larger mean and standard deviation than the entire grid for both the background data and the off-target data suggesting edge effects along the right-hand edge. In order to keep the target centered within the measurement domain, the grid was reduced by 5 rows/columns around the entire grid. The new measurement domain (referred to as the reduced grid) of 21 rows and 27 columns with 567 observations is illustrated by the heavy black rectangle in Figure 14. The mean and variance of the reduced grid is presented in Table 5.

When comparing data sets, it is sometimes beneficial to standardize the data. Standardized data directs focus to its underlying features, while preserving its distribution. Both data sets (background and with target) are standardized according to,

$$Z = \frac{V_i - \mu_V}{\sigma_V} \quad for\ i = 1,2, \dots N \tag{4}$$

where, $Z,$ = standardized velocity, $V_i$ = velocity at each point, $N$ = scalar observations, $\mu_V$ = mean of velocity vector, subscript $V$ = velocity vector made up of $N$ observations, and $\sigma_V$ = standard deviation of the velocity vector. Using the data on a reduce grid the mean and standard deviation of the background data was calculated for each frequency and is shown in Figure 15. It is interesting to note that the mean and standard deviation changes very little over this frequency band. This suggest that the acoustic excitation is at sufficiently long wavelengths with respect to soil heterogeneity to provide a uniform excitation of the surface. The origin of the peaks in this figure are unknown but is most likely associated with modes in the sand box. The peak at 60Hz and 180 Hz may be a result of electrical noise. The standardization for the data with the target uses a subset of the data which excludes data over the target or what we described earlier as off-target data. The mean and standard deviation of the off-target data is also presented in Figure 15. Each data set is standardized according to equation (4) with a unique value for the mean and standard deviation for each frequency. The spectrogram of the standardized velocity for a point

16

on target, off target and background data is shown in Figure 16. Comparing the standardized

spectrogram (Figure 16) to the spectrogram of the original data (Figure 3) indicates that the

structure of the data is unchanged.

The standardize background data (Figure 17A) has a mean zero and variance of 1. The

standardized velocity with a buried target (Figure 17B) has a mean of 0.88 and the variance is

27.4 because the data was standardized using the mean and standard deviation of the off-target

data. The two data sets from data conditioning and geostatistical methods include the

standardized data sets on a reduced grid of background velocity and the velocity with a target

present.

# IV. RESULTS AND DISCUSSION

## GEOSTATISTICAL RESULTS

Standardizing data should result in a data set with a mean-zero with a variance of 1. The standardized velocity with a buried target resulted has a mean of 0.88 and the variance is 27.4 because the standardization was performed using the off-target velocities only. As a check on the standardization, the variograms were calculated for the background data and off-target data. To allow for equivalent data sets, some points (at the equivalent location of the target) were removed the background velocity. The spatial velocity maps for the background (Figure 18A) and the off-target data (Figure 18B) have the same number of points and spatial distributions. The number of pairs as a function of separation distance for these data sets are shown in Figure 19. The irregularity in number of pairs versus separation distance is associated with the uneven sampling in the x and y directions. The number of pairs start to decrease for separation distances great than 40cm. A range of 40 cm and a total number of 20 lags is applied in the geostatistical calculations. The variograms for the background and off target (Figure 20) are comparable confirming the standardization is correct.

A geostatistical analysis of the spatial distribution of the ground surface velocity excited by a loudspeaker without a buried target (Figure 17A) and with a buried target (Figure 17B) were conducted on the standardized data for an excitation of 64Hz. Both data sets have the same number of points and spatial distribution. A stacked histogram of the background velocity and

18

the velocity with the target is displayed in Figure 21. The majority of the data are located around the zero mean since the target anomaly only effects a small area of the domain. The larger standardized velocities are associated with the high velocities over the buried target. The number of pairs versus separation distance for both data sets is shown in Figure 22. The total number of pairs is 161,028. The analysis using SGeMS indicated that anisotropy was not prevalent in the data, so omnidirectional variograms were constructed in Matlab.

The variograms (Figure 23) show the dramatic effects of a buried target. The background velocity asymptotes to the variance in the variogram at a separation distance of 3 cm, which indicates that no correlation at scales beyond 3cm. Uncorrelated background velocity suggest that the response is comparable to an uncorrelated random field of white noise, until an anomaly (i.e., buried target) is positioned in the domain. The uniformity of the background velocity also indicates that if any modes are excited in the sand box the resulting velocity field is below the natural variability.

The buried target introduces much higher variability, relative to the surrounding points, and disrupts the random, uncorrelated response of the background. The resulting target induced variability is subjective, which relies on target location in the grid. Variograms for the with-target response reveal a variance line that is roughly 27X the variance of the background velocity and has irregular structural features (Figure 23). The variogram of crosses the total variance (27) at a separation distance of about 8 cm suggesting off-target points at distances beyond 8 cm in separation begin to react with the target, thus increasing variability. The variogram shows sill-like structure of magnitude 35 at a separation distance of 12cm and a magnitude of 45 at a separation distance of 18cm. The variogram is trying to reach a correlation length at the sill-like structure at 12 cm and 18 cm, respectively; however, the continuous interaction between the

19

target and more distant off-target points increases the variability to a maximum value of 54 at a separation distance of 25 cm. The most points are paired between 25cm and 35 cm, where the edges of the data conditioned measurement grid are located between 25 and 35 cm from the center of the target at highest resonance. The importance of the peak at 25 cm corresponds with the distance from the target to the points near the edges of the grid. If a 25 cm radius is placed around the target, the most pairs are located at that distance (due to the asymmetrical grid dimension), which also corresponds to the edges of the domain. Beyond 25 cm, the variogram retreats, suggesting that less points at greater distances interact with the target, and more off-target points are interacting with one another, causing variability to decrease. The separation distance should correspond to unique characteristics dimensions of the velocity field. Some possibilities include the location of the target within the domain, the width of the anomaly (related to target size and depth of burial), and the distanced between sampled points. The magnitude of the variogram may be dependent on the magnitude of the target anomaly. The influence of the target location was explored in the sensitivity analysis.

DATA SENSITIVITY

To investigate the effect of location of the target within the measurement domain, a subdomain is selected and moved around. Frames situated around the data conditioned grid challenge the previous interpretations of variogram structure. In each case, the subdomain has the same number of rows and columns but the target is located in a different position within the subdomain (Figure 24). With irregular sample spacing, it is apparent that the subdomains have unequal dimensions, but an equal number of points. The frames in the bottom edges contain slightly more pairs per separation distance due to the smaller spatial sampling as compared to the

top left and right corners (Figure 25). It is assumed that this small difference in pairs is not important.

The variograms for the different subdomains shown in Figure 24 are plotted in Figure 26. Each subplot contains the variogram with a new target location and the variogram with the target centered in the subdomain as a reference. Effects of reducing the measurement domain can be observed by comparing then the variogram with the target centered in the subdomain (red points) in Figure 26 to the variogram of the completed measurement domain (Figure 23). Reducing the measurement domain cause to the magnitudes of the variogram to increase. The center frame variogram follows a similar structure as the with-target variogram, but at different distances. Encounters between off-target and on-target points within a 17 – 20 cm radius around the target show that the extent of the greatest number of pairs occur in this range. The variogram cross the variance line at approximately the same separation distance of 8cm, the sill-like feature a separation distance of 12cm, and the peak of the variogram has now moved to about 18cm. The sill like feature at 18cm is either not present or is merged with the peak in the variogram. Moving the target from right to left in the subdomain (compare Figure 26A and Figure 26B or Figure 26C and 26D) produces the same variograms up to a separation distance of about 10cm. The sill-like feature at 12cm also appears to be at the same location for the targets located in upper parts of the subdomain but is moved to slightly lower separation distances the target located in the lower part of the subdomain.

The variograms with the target off center appear to have two peaks. It is postulated that this could be associated with different distances from the boundary of the domain in the x and y directions and requires further investigation. This analysis suggests that the maximum (or two peaks) are associated with distances of the target in the measurement domain. The peaks seen in

the top and bottom frames are a product of the distanced from the center of the target to the edge of the grid in the x- and y-direction. Since the variograms are calculated as omnidirectional, the peaks are a combination of the distances from the edges to the target in all directions. The first two peaks in all frames correlate with the shortest distances from the edges to the center of the target, while those at farther separation distances correlate with the longer distances. Moving the frame to place the target location in the corners of the grid ultimately suggest that the structure of the variogram becomes unstable, but is still preserved.

Optimizing data acquisition and survey speeds in the field depend on the spatial sampling. In order to evaluate the dependence of the variogram of the spatial sampling the data is decimated and the geostatistical analysis is performed. New measurement grids (Figure 27) were obtained by removing every second and third point. This yielded a total number of 154 observations when every second point removed, and 63 when every third removed. The number of lags was reduced, while the lag spacing was increased, to better fit the new spacing between observations. The number of pairs per separation distance fluctuate at greater distances, as there is unequal spacing between observations between the rows and columns. There are 11,935 pairs when every second point was removed and 2,016 pairs when every third point was removed (Figure 28A). With every other observation removed from the data, the number of pairs per separation distance becomes very unstable; however, the variogram displays structural features previously observed in the full grid. When every third point is removed, the variability between pairs roughly follows the same structure. The variogram for every second point removed depicts a similar structure to the data with the entire data set. When every third point is removed, the variogram becomes more erratic, with large jumps in variogram values at both small and large separation values (Figure 28B). The peaks appear to be moved to 27 cm, which indicates that

because the lag spacing was adjusted, pairs between off-target and on-target points influence the variability most at that distance.

The robustness of the variogram behavior on the signal to noise was studied by increasing the noise floor of the data. Noise generated with mean 0 and different variances replaced the off-target observations whereas the target resonance stayed the same because it was assumed the target would respond equivalently to white noise. The generated noise had variances that of 29.7, 121, 233, 316, and 438. Velocity maps displayed the visual effects of added noise on the measurement grid (Figure 29). The target anomaly is visible with the addition of higher levels of noise. The respective variograms are displayed in Figure 30. Based off visual inspection, the velocity maps indicate the presence of the target. Alternatively, the structure of the variogram associated with a buried target was lost when the variance of the of the added noise reached 438. At a high variance relative to the with-target variance of 27.4, the surrounding variability masks the geostatistical characteristics of the target placed within the measurement grid. This suggest that the variogram structure is not as robust as simple visual inspection of the velocity map for detecting buried targets.

In an additional simulation, random fields with internal correlation lengths replaced off-target observations. The influence of correlated noise on the variogram structure was consisted of generating ten random fields with fixed correlation lengths using a code supplied by Dr. Robert Holt, (Appendix B), to replace the off-target observations. They were produced with different variances and increasing correlation lengths of 6, 15, and 30 cm (Figure 31 – 32, respectively). The random fields had an exponential covariance structure, with a mean of 0 and variances of 10, 20, 30, 40, 50, 70, 100, 200, 300, and 400. When the off-target points were replaced with the random field, the variances changed with the addition of the target. For example, in the

variogram for a random field (RF) with correlation length of 6 cm (Figure 31), random field 4 (RF4) originally had a variance of 40, but the addition of the target increased it to 60.1. This is similar to when RF5 should have a variance of 50. The variance of RF6 is 71.2, where the random field had a variance of 70. The presence of the target influences the variances up to that point, then the target signature is overcome by surrounding variability. Furthermore, the variogram structure is routinely preserved through all correlation lengths up to a variance of about 70 when the correlation length is 6 cm. Multiple scales of correlation can be seen in the variogram, where shoulders develop on the leading edge, but the resonance of the target still dominates the structure.

When the correlation length is increased to 15 cm (Figure 32), the target influence declines at variance smaller than the correlation length of 6 cm. A correlation length of 15 cm is similar to the dimension of the target. At RF3 on the variogram, the variance of the random field should be 30. After the target is included, the variance increases to 48.8. At this point, the target and the correlation length are of similar size and the variogram may not be a valid indicator of target presence. As variability of the random field increases to 40, the variance drops and the target signature is masked by the surrounding variability. This concept follows through to a variance of 400, where the structure of the with-target variogram is lost and the variogram values follow the variance and correlation length of the RF.

At a correlation length of 30 cm (Figure 33), almost twice the size of the target, the variograms do not indicate a correlation length of 30 cm until RF7, when the variance should 100. RF7 lies under the average, and it considered the extent of where target variogram characteristics exist. Higher variances, such as RF9 and RF10, do not reach their calculated variances of 300 and 400, respectively. It was assumed that calculating a RF with high variances

24

in a small domain of 567 points and a correlation length of 30 cm, caused the variances to behave oddly. The domain is small compared to the correlation length of 30 cm, and not enough sampled points exist for the data to assume ergodicity. RF8 to RF10 develop a trend that is equal to the fixed correlation length of 30 cm.

A linear trend was added to the standardized velocity data to observe the effects on spatial variability. The purpose of integrating a trend is to simulate field parameters. The descending trend is in the southeast direction. The fields are generated with increasing variances. Velocity maps suggest that the target resonance is still visible at its original location (Figure 34 and 35). Scales of the velocity maps differ between one another to show the distribution of the values relative to the target. Variograms were constructed from the trended data added across the measurement grid and are presented in Figure 36. the variograms indicate that incorporating trended data with high variances relative to the target mask the target signature in the variogram.

Aside from the frequency value of 64 Hz previously evaluated, Figure 37 depicts additional frequency on the spectrogram for a point on top of the target. These frequencies include: 40 Hz, 92 Hz, 128 Hz, and 180 Hz. The velocity map at 40 Hz and 92 Hz does not show a target signature, along with the variogram (Figure 38 and 39). These variograms behave similarly to the background and off-target points, where high variability is not present. The variograms appear to asymptote to a variance of 1, but the with-target variogram masks small-scale variability present and considered it negligible in comparison. Although it was a lower contrast compared to 64 Hz, the visibility of it confirmed that the target has resonance correlation to a different frequency. At 128 Hz, the target is visible in the velocity map (Figure 40A) but the variogram is of overall lower magnitude (Figure 40B). The variance at 128 Hz is 7.04. The second highest target resonance is at 128 Hz. This may be a result of harmonics resonance

specific to the type of target used in the experiment. The velocity map and variogram at 180 Hz are comparable to those at 52 Hz and 92 Hz (Figure 41); however, a small cluster is visible in the velocity map at the target location.

# V. SUMMARY AND CONCLUSION

A Polytec LDV system measured background velocity and velocity with a buried target present in a confined wooden box filled with sand. The measured grid had a trapezoidal shape with a height of 83.1 cm, and top and bottom length of 96.5 cm and 71.1 cm. The raw data sets from Polytec produced complex velocity vectors of 1147 points through a band of 40 – 400 Hz with steps of 4 Hz.

A data conditioning process resulted in a reduced grid of standardized velocity points for both the background velocity and the velocity with a target present. The geostatistical analysis performed after the data conditioning identified characteristics of each of the data sets. The standardized background velocity was mean zero with a variance of 1. The background velocity variogram asymptotes to zero and the variogram asymptotes to the overall variance fairly quickly, which indicates that there is no correlation at larger distances. Uncorrelated background velocity suggest that the response is comparable to an uncorrelated random field of white noise, until an anomaly (i.e., buried target) is positioned in the domain. The uniformity of the background velocity also indicates that if any modes are excited in the sand box the resulting velocity field is below the natural variability.

The velocity with a buried target exhibits a variance 27X larger than the background velocity because it was standardized by the off-target data to avoid influence from target response. The target produces clearly identifiable changes in the variogram. The buried target introduces higher variability relative background, and disrupts the random, uncorrelated response of the background. The resulting target induced variability is subjective, which relies on target location in the grid. The shape of the variogram and the position of peaks in the variogram depend on the location of the target within the measurement domain. When the target is centered within the measurement domain, the variogram peak occurs at a separation distance equivalent to the average distance from the center of the target to the edge of the domain. When the target is off center within the measurement domain, two peaks occur, reflecting the distances from the center of the target to the near and far edges of the measurement domain. The width of the target response above the sill in the variogram generally reflects the width of the target response in the domain.

Sensitivity studies were conducted to evaluate the impact of fewer data and uncorrelated, correlated, and trending noise in the off-target soils. As data were decimated from 567 points to 154 points and 63 points, the structure of the target signature in the variogram was preserved with 154 points and substantially reduced with 63 points, indicating that the sample spacing must be sufficiently dense to allow a number of samples to encounter the target. When uncorrelated noise replaced off-target observations, the target is interpretable from the variogram up to a variance of over 400. Alternatively, when a random field with internal correlation lengths is applied, the target is obscured at higher variances and higher correlation lengths. Similarly, strong trends in the background obscure the target.

This study suggests that understanding the spatial structure of the acoustic response of natural soils is critical to the development of land mine detection technologies using an LDV. Future studies should focus on collecting experimental data from field sites. Emphasis should be placed on understanding the types and magnitude of natural acoustic variability within a variety of soil types and soil conditions (e.g., roads versus fields). Soil moisture content and vertical heterogeneity within the soils may exert substantial influence on the acoustic response of natural soils and can readily be incorporated into future geostatistical analyses. The natural variability in the acoustic response should be determined and cataloged for a variety of soil types and conditions and compared with target responses within the same soils.

REFERENCES

ARANCHUK, V., SABATIER, J.M., and ALBERTS II, W.C.K., 2006, Acoustic detection

of buried landmines using pulsed ESPI: Society of Photo-Optical Instrumentation Engineers, v.

45, p. 10–17, doi: 10.1117/1.2358975.


ARNOTT, W.P., and SABATIER, J.M., 1990, Laser-Doppler vibrometer measurements of acoustic

to seismic coupling: Applied Acoustics, v. 30, p. 279–291, doi: 10.1016/0003-682X(90)90078-9.


BARNES, R.J., 1988, Bounding the required sample size for geologic site characterization:

Mathematical Geology, v. 20, p. 477–490, doi: 10.1007/BF00890332.


BASS, H.E.,et al., 1980, Coupling of airborne sound into the earth: Frequency dependence: The

Journal of the Acoustical Society of America, v. 67, p. 1502–1506, doi: 10.1121/1.384312.


BIOT, M.A., 1956, Theory of propagation of elastic waves in a fluid-saturated porous solid. II:

Higher frequency range: The Journal of the Acoustical Society of America, v. 28, p. 179–191,

doi: 10.1121/1.1908241.


BRUS, D.J., and DE GRUIJTER, J.J., 1997, Random sampling or geostatistical modelling?

Choosing between design-based and model-based sampling strategies for soil (with discussion):

Geoderma, v. 80, p. 1–44, doi: 10.1016/S0016-7061(97)00072-4.

BURGESS, T.M., and WEBSTER, R., 1980, Optimal interpolation and isarithmic mapping of soil

properties, I. The semivariogram and punctual kriging: Journal of Soil Science, v. 31,    p. 315–

331, doi: 10.1111/j.1365-2389.1980.tb02084.x.


BURGESS, T.M., WEBSTER, R., MCBRATNEY, A.B., 1981, Optimal interpolation and isarithmic

mapping of soil properties, IV. Sampling strategy: Journal of Soil Science, v. 32, p. 643– 659,

doi: 10.1111/j.1365-2389.1981.tb01737.x.


DONSKOY, D., EKIMOV, A., SEDUNOV, N., AND TSIONSKIY, M., 2002, Nonlinear seismo-acoustic

land mine detection and discrimination: The Journal of the Acoustical Society of America, v.111,

p. 2705–2714, doi: 10.1121/1.1477930.


HARROP, N., and ATTENBOROUGH, K., 2002, Laser-Doppler vibrometer measurements of

acoustic-to-seismic coupling in unconsolidated soils: Applied Acoustics, v. 63, p. 419– 429, doi:

10.1016/S0003-682X(01)00042-1.


HICKEY, C.J., and SABATIER, J.M., 1997, Measurements of two types of dilatational

waves in an air-filled unconsolidated sand: The Journal of the Acoustical Society of America, v.

102, p. 128–136, doi: 10.1121/1.419770.


ISAAKS, E.H., and SRIVASTAVA, R.M., 1989, An Introduction to Applied Geostatistics: Oxford

University Press, New York, 561 p.

JARDETZKY, W.S., and PRESS, F., 1952, Rayleigh-wave coupling to atmosphere compression

waves: Bulletin of the Seismological Society of America, v. 42, p. 135–144.

KORMAN, M.S. and SABATIER, J.M., 2004, Nonlinear acoustic techniques for landmine detection:

Journal of Acoustical Society of America, v. 116, p. 3354–3369, doi: 10.1121/1.1814119.

KRIGE, D.G., 1951, A statistical approach to some basic mine valuation problems on the

Witwatersrand: Journal of the Chemical Metallurgical and Mining Society of South Africa, v. 52,

p. 119–139.

LAMB, H., 1904, On the propagation of tremors over the surface of an elastic solid: Philosophical

Transactions of the Royal Society A: Mathematical, Physical, and Engineering Sciences, v. 203,

p. 1–42, doi: 10.1098/rsta.1904.0013.

MATHERON, G., 1963, Principles of geostatistics: Economic Geology, v. 58, p. 1246–1266, doi:

58.8.1246.

MUIR, T.G., COSTLEY, R.D., SABATIER, J.M., 2014, Comparison of acoustic and seismic

excitation, propagation, and scattering at an air-ground interface containing a mine-like

inclusion: Acoustical Society of America, v. 135, p. 49–57, doi: 10.1121/1.4835895.

OLIVER, M., WEBSTER, R., GERRARD, J., 1989, Geostatistics in physical geography, Part I: Theory, Transactions of the Institute of British Geographers, v. 14, p. 259–269, doi: 10.2307/622687.

PRESS, F., and EWING, M., 1951a, Ground roll coupling atmospheric to compressional waves: Geophysics, v. 16, p. 416–430, doi: 10.1190/1.1437684.

PRESS, F., and EWING, M., 1951b, Theory of air-coupled flexural waves: Journal of Applied Physics, v. 22, p. 892–899, doi: 10.1063/1.1700069.

PRESS, F., and OLIVER, J., 1955, Model study of air-coupled surface waves: The Journal of the Acoustical Society of America, v. 27, p. 43–46, doi: 10.1121/1.1907494.

SABATIER, J.M., BASS, H.E., BOLEN, L.N., ATTENBOROUGH, K., 1986a, The interaction of airborne sound with the porous ground: The theoretical formulation: The Journal of the Acoustical Society of America, v. 79, p. 1345–1352, doi: 10.1121/1.394058.

SABATIER, J.M., BASS, H.E., BOLEN, L.N., ATTENBOROUGH, K., 1986b, Acoustically induced seismic waves: The Journal of the Acoustical Society of America, v. 80, p. 646–649, doi: 10.1121/1.394058.

SABATIER, J.M., and XIANG, N., 2001, An investigation of acoustic-to-seismic coupling to detect buried antitank landmines: IEEE Transactions on Geoscience and Remote Sensing, v. 39, p. 1146–1154, doi: S0196-2892(01)05112-9.

SCOTT, W.R., MARTIN, J.S., and LARSON, G.D., 2001, Experimental model for a seismic landmine detection system Institute of Electrical and Electronics Engineers Geoscience and Remote Sensing, v. 39, p. 1155–1164, doi: 10.1109/36.927432.

SCRUBY, C.B., and DRAIN, L.E., 1990, Laser Ultrasonics Techniques and Applications: Adam Hilger, Bristol/Philadelphia/New York, 467 p.

WEBSTER, R., 1985, Quantitative spatial analysis of soil in the field: Advances in Soil Science, v. 3, p. 1–70, doi: 10.1007/978-1-4612-5090-6_1.

XIANG, N., and SABATIER, J.M., 2003, An experimental study on antipersonnel landmine detection using acoustic-to-seismic coupling: Acoustical Society of America, v. 113, p. 1333–1341, doi: 10.1121/1.1543554.

XIANG, N., and SABATIER, J.M., 2004, Laser-Doppler vibrometer-based acoustic landmine detection using the fast M-sequence transform: Institute of Electrical and Electronics Engineers Geoscience and Remote Sensing Letters, v. 1, p. 292–294, doi: 10.1109/LGRS.2004.836257.

TABLES

| Entire Raw Data Sets (1147 points) | | | |
|---|---|---|---|
| | Background | Off Target | With Target |
| Mean (m/s) | 5.78E-05 | 6.66E-05 | 7.88E-05 |
| Variance ($m^2/s^2$) | 6.23E-10 | 4.23E-08 | 5.25E-08 |

Table 1. Mean and variance of initial velocity data.

| Data with Outlier Replacement (1147 points) | | | |
|---|---|---|---|
| | Background | Off Target | With Target |
| Mean (m/s) | 5.76E-05 | 5.9E-05 | 7.15E-05 |
| Variance ($m^2/s^2$) | 5.83E-10 | 9.7E-10 | 1.21E-08 |

Table 2. Mean and variance of velocity data with outliers replaced.

| Background | | | | |
|---|---|---|---|---|
| Row | 1 to 5 | 6 to 10 | 22 to 26 | 27 to 31 |
| Mean (m/s) | 5.75E-05 | 5.86E-05 | 5.65E-05 | 5.60E-05 |
| Variance ($m^2/s^2$) | 5.16E-10 | 6.40E-10 | 5.80E-10 | 5.67E-10 |
| Means Ratio | 1.00 | 1.02 | 0.98 | 0.97 |
| Variance Ratio | 0.89 | 1.10 | 1.00 | 0.97 |
| Off Target | | | | |
| Row | 1 to 5 | 6 to 10 | 22 to 26 | 27 to 31 |
| Mean (m/s) | 6.96E-05 | 6.05E-05 | 5.06E-05 | 5.89E-05 |
| Variance ($m^2/s^2$) | 1.17E-09 | 8.67E-10 | 5.78E-10 | 9.94E-10 |
| Means Ratio | 1.18 | 1.02 | 0.86 | 1.00 |
| Variance Ratio | 1.20 | 0.89 | 0.59 | 1.02 |

Table 3. Background and off-target velocity mean and variance with respective ratios of the sectioned rows to the entire grid.

| Background | | | | | | |
|---|---|---|---|---|---|---|
| Column | 1 to 5 | 6 to 10 | 11 to 15 | 23 to 27 | 28 to 32 | 33 to 37 |
| Mean (m/s) | 6.75E-05 | 6.18E-05 | 5.60E-05 | 5.40E-05 | 5.58E-05 | 5.49E-05 |
| Variance ($m^2/s^2$) | 8.26E-10 | 6.35E-10 | 4.79E-10 | 5.05E-10 | 5.05E-10 | 5.96E-10 |
| Means Ratio | 1.17 | 1.07 | 0.97 | 0.94 | 0.97 | 0.95 |
| Variance Ratio | 1.42 | 1.09 | 0.82 | 0.87 | 0.87 | 1.02 |
| Off Target | | | | | | |
| Column | 1 to 5 | 6 to 10 | 11 to 15 | 23 to 27 | 28 to 32 | 33 to 37 |
| Mean (m/s) | 6.31E-05 | 5.73E-05 | 5.94E-05 | 5.77E-05 | 5.89E-05 | 5.64E-05 |
| Variance ($m^2/s^2$) | 1.27E-09 | 9.20E-10 | 1.03E-09 | 9.59E-10 | 7.67E-10 | 9.44E-10 |
| Means Ratio | 1.07 | 0.97 | 1.00 | 0.98 | 1.00 | 0.95 |
| Variance Ratio | 1.30 | 0.94 | 1.06 | 0.98 | 0.79 | 0.97 |

Table 4. Background and off-target velocity mean and variance with respective ratios of the sectioned columns to the entire grid.

| Data with Outlier Replacement on a Reduced Grid | | | |
|---|---|---|---|
| | Background | Off Target | With Target |
| Mean (m/s) | 5.63E-05 | 5.61E-05 | 8.12E-05 |
| Variance ($m^2/s^2$) | 5.22E-10 | 8.46E-10 | 2.32E-08 |

Table 5. Mean and variance of the data on a reduced grid.

FIGURES

A)



B)



Figure 1. Experimental set-up and buried object. A) Wooden box filled with playground sand, tripod with Vibrometer scanning head and loud speaker as an excitation source; B) Object to be buried.
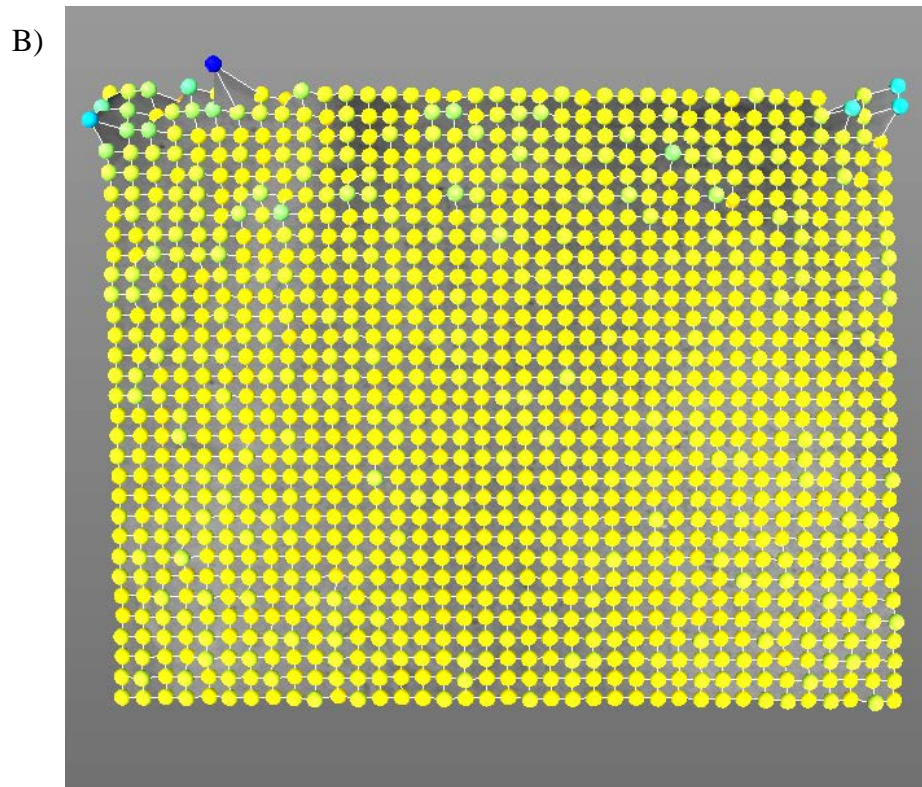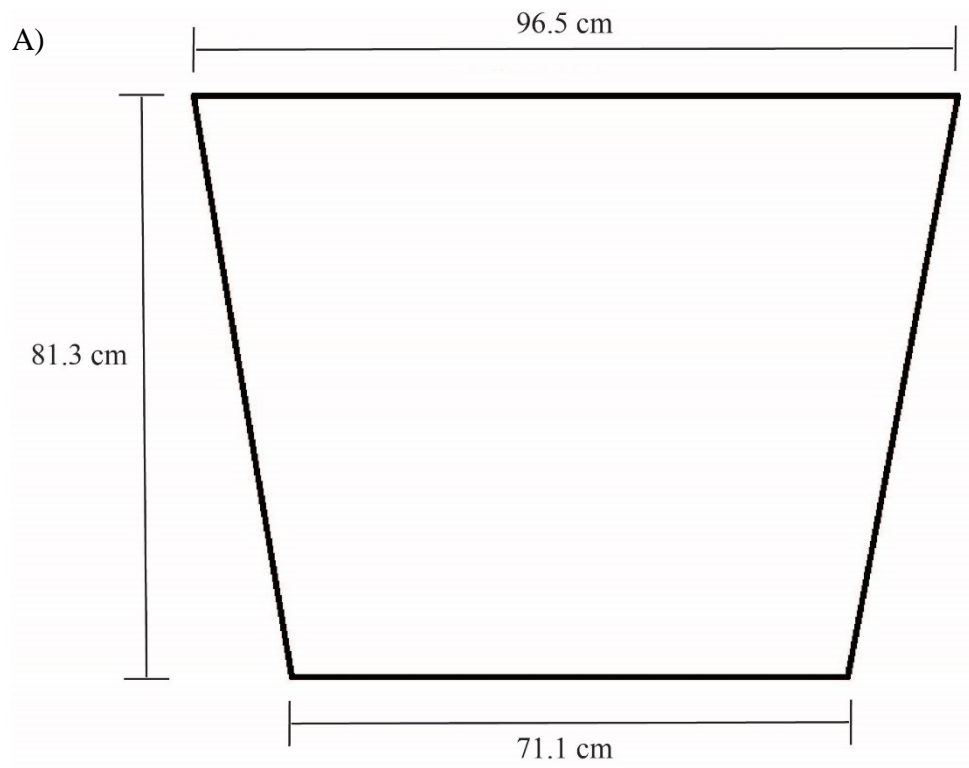
Figure 2. A) Actual scanned area on sandbox; B) Display of measurement points in Polytec

software.
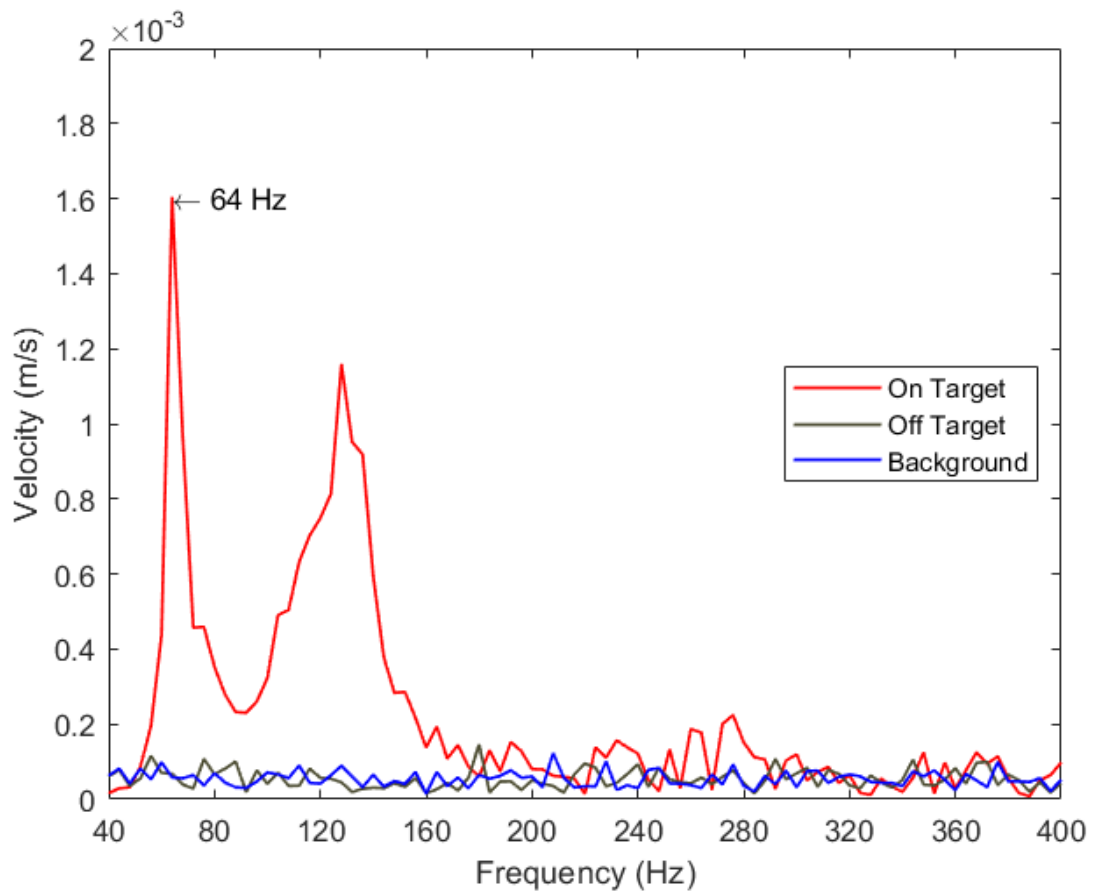
Figure 3. Spectrogram of velocity for points on and off target and background velocity as a function of frequency. The highest target resonance is at 64 Hz. Subsequent geostatistical analysis will be performed on data at 64Hz.
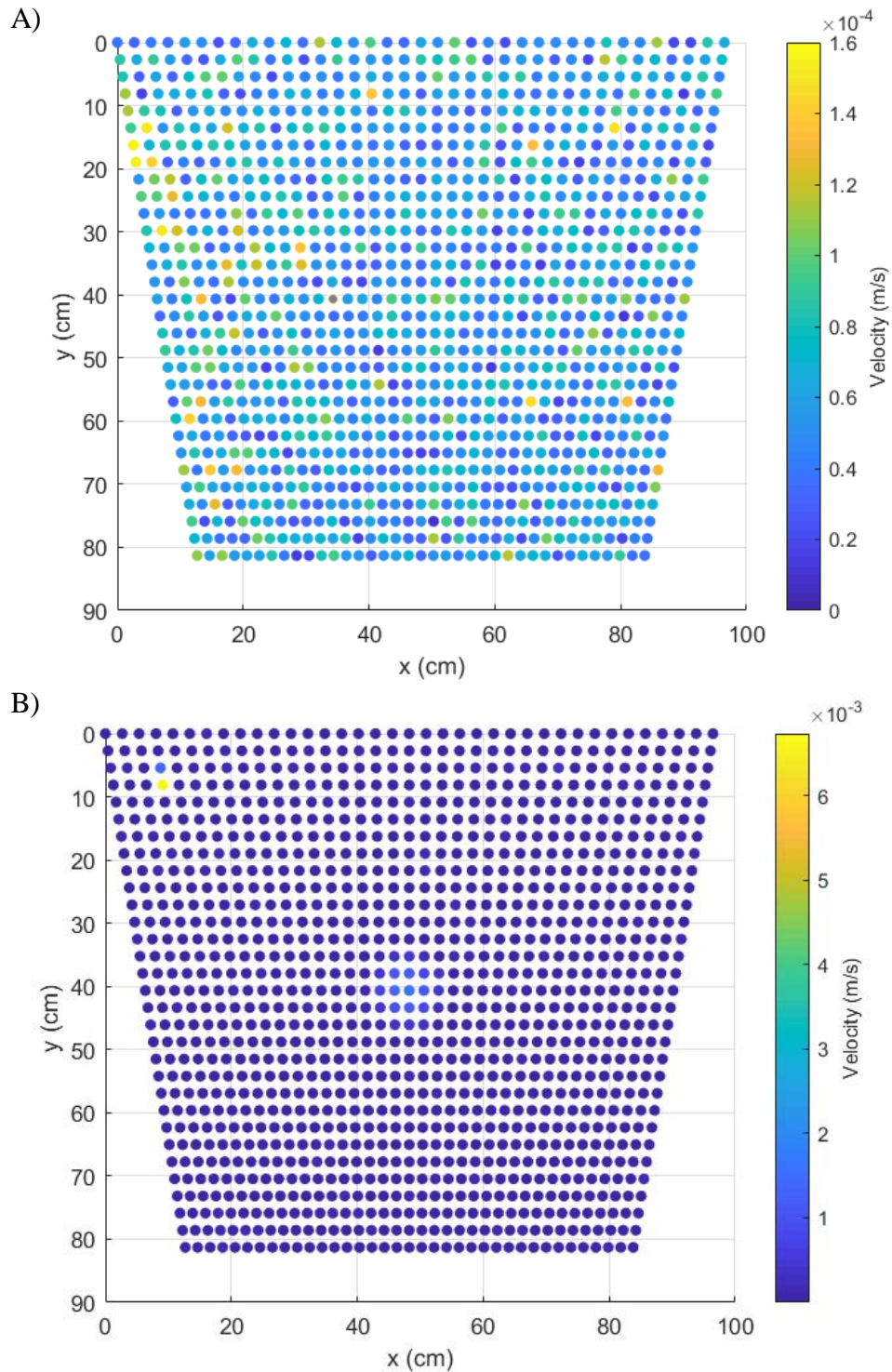
Figure 4. Velocity maps at 64 Hz for: A) background velocity; B) velocity data with a target present. The target response is masked by outlier spikes.

Note: Velocity scales differ to show distribution of values.
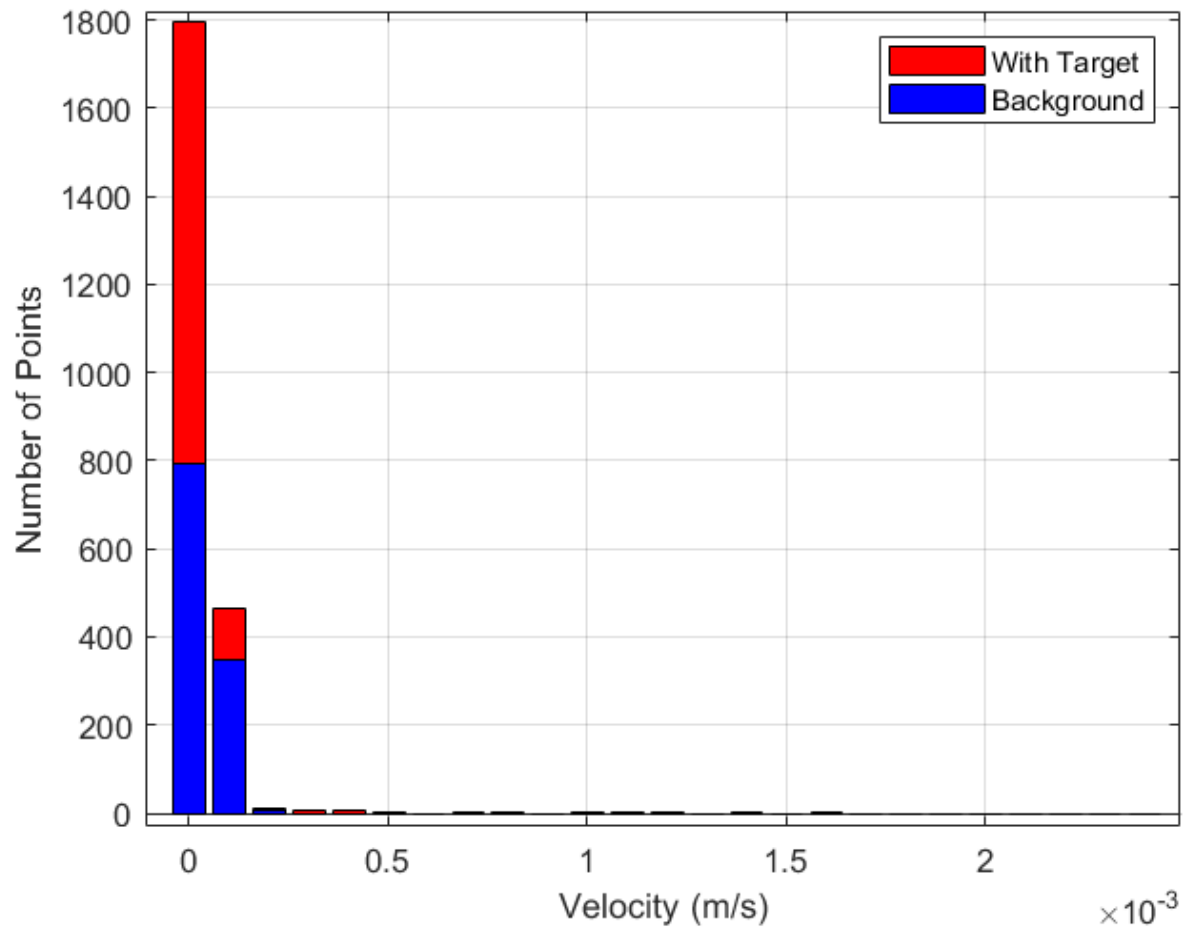
Figure 5. Stacked histogram of the entire raw data sets (1,147 points) of the background velocity (blue) and the velocity with a target (red).
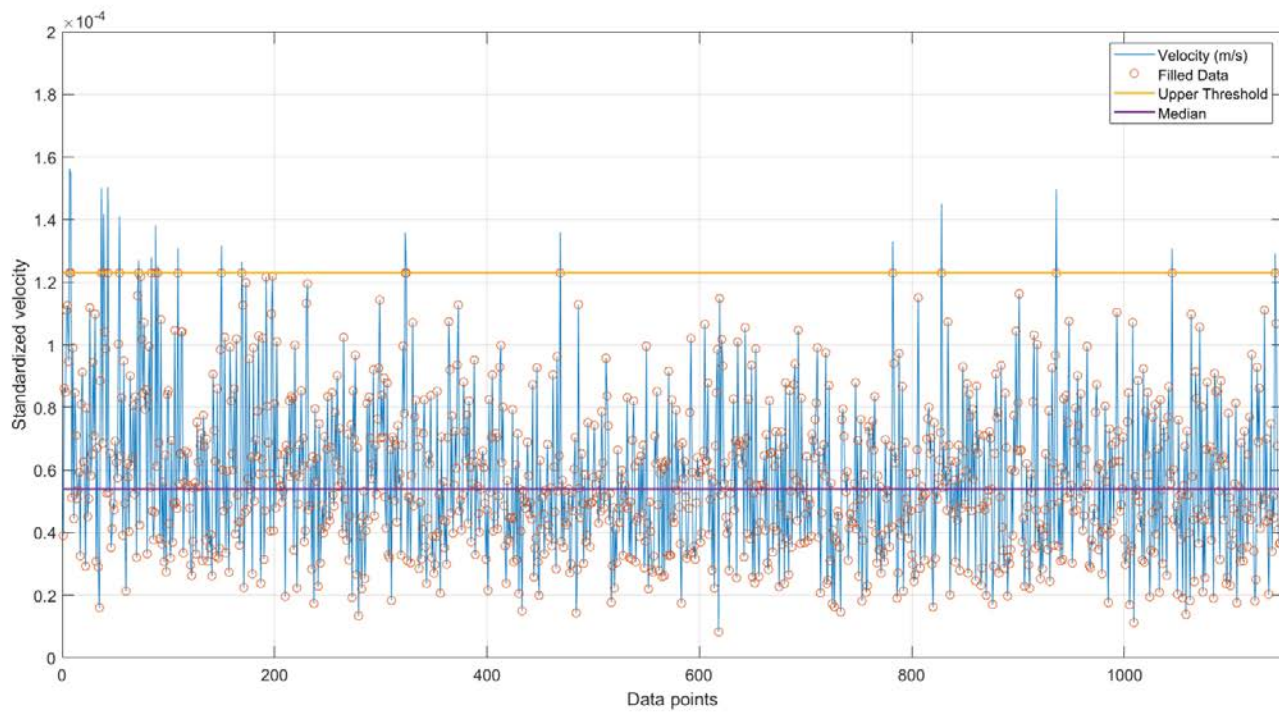
Figure 6. Process of outlier replacement using the MAD method for background velocity.
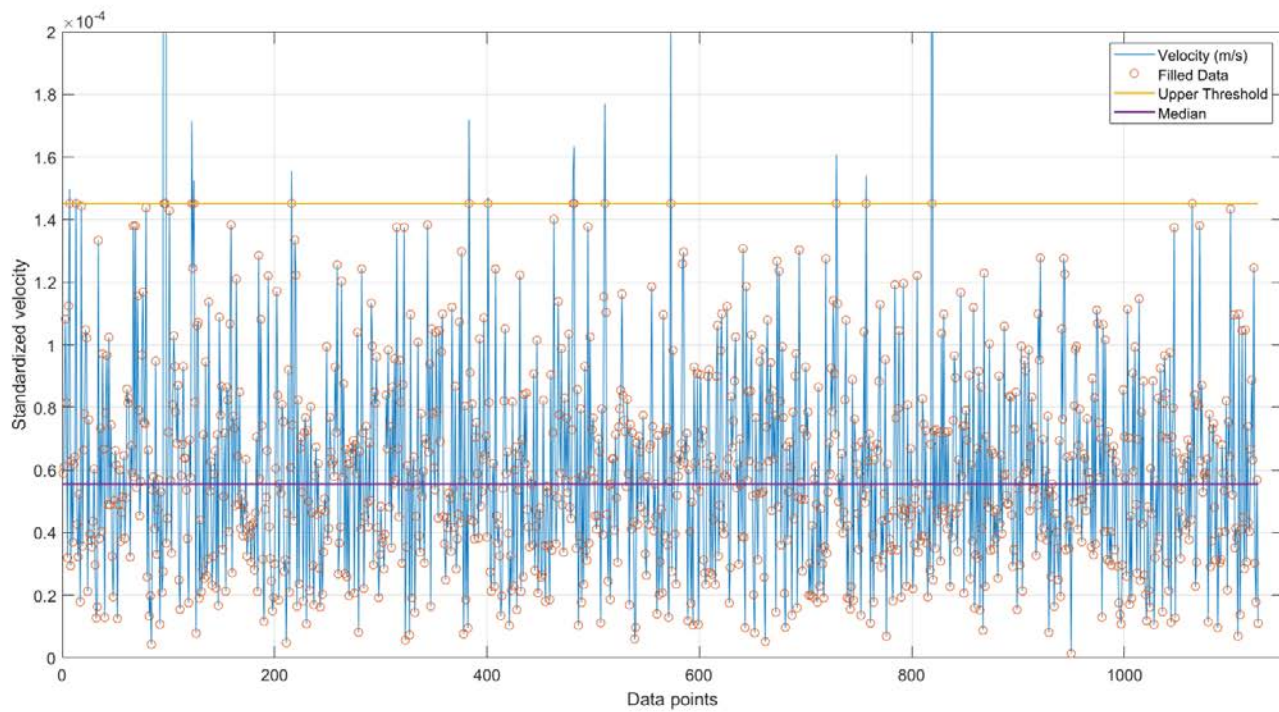
Figure 7. Process of outlier replacement using the MAD method for the velocity data off target. The extended high velocity spikes are an artifact of LDV speckle.
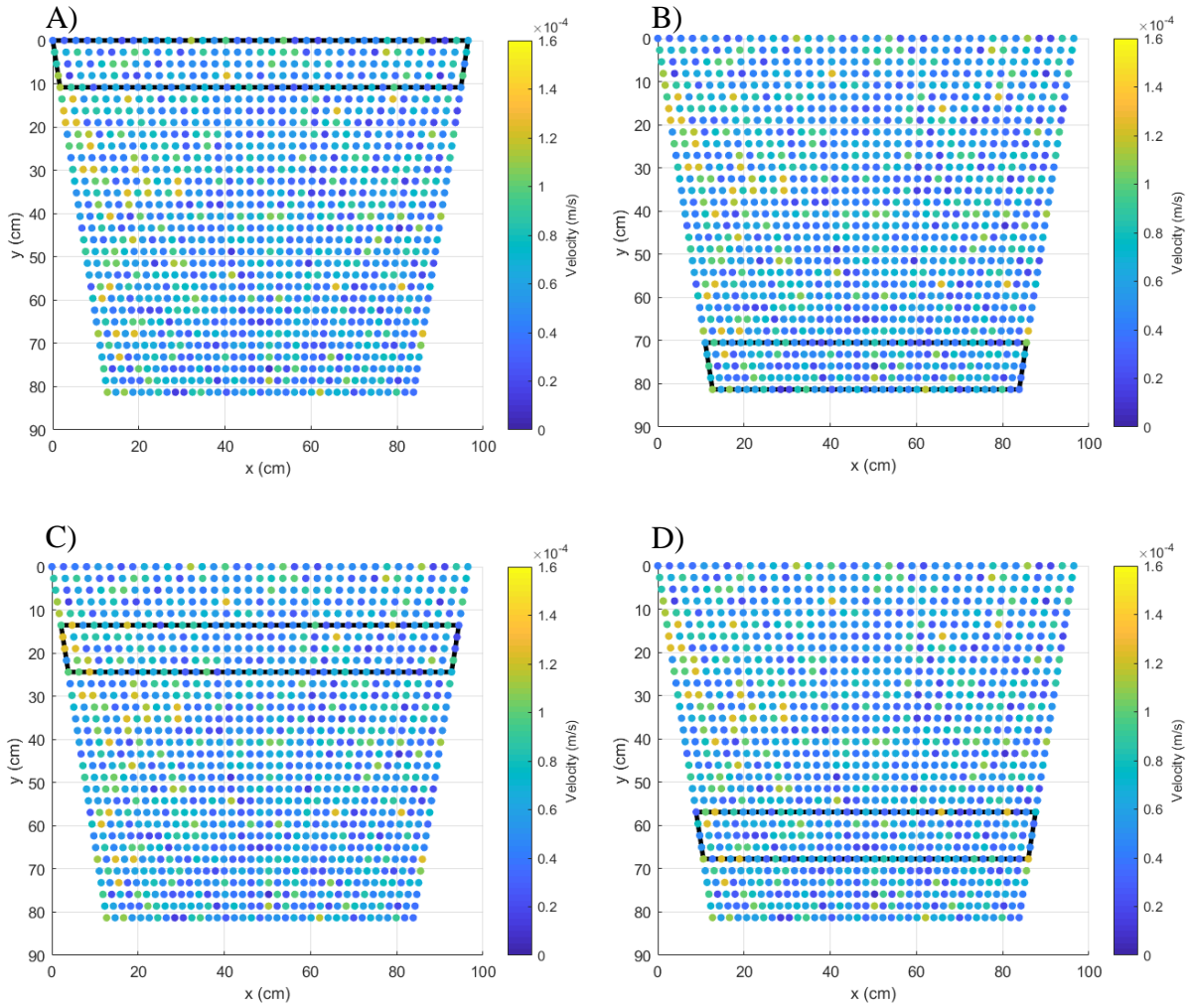
Figure 8. Velocity maps of top and bottom edges of the background. A) Top edge rows 1 to 5; B) Top edge rows 6 to 10; C) Bottom edge rows 22 to 26; D) Bottom edge rows 27 to 31.
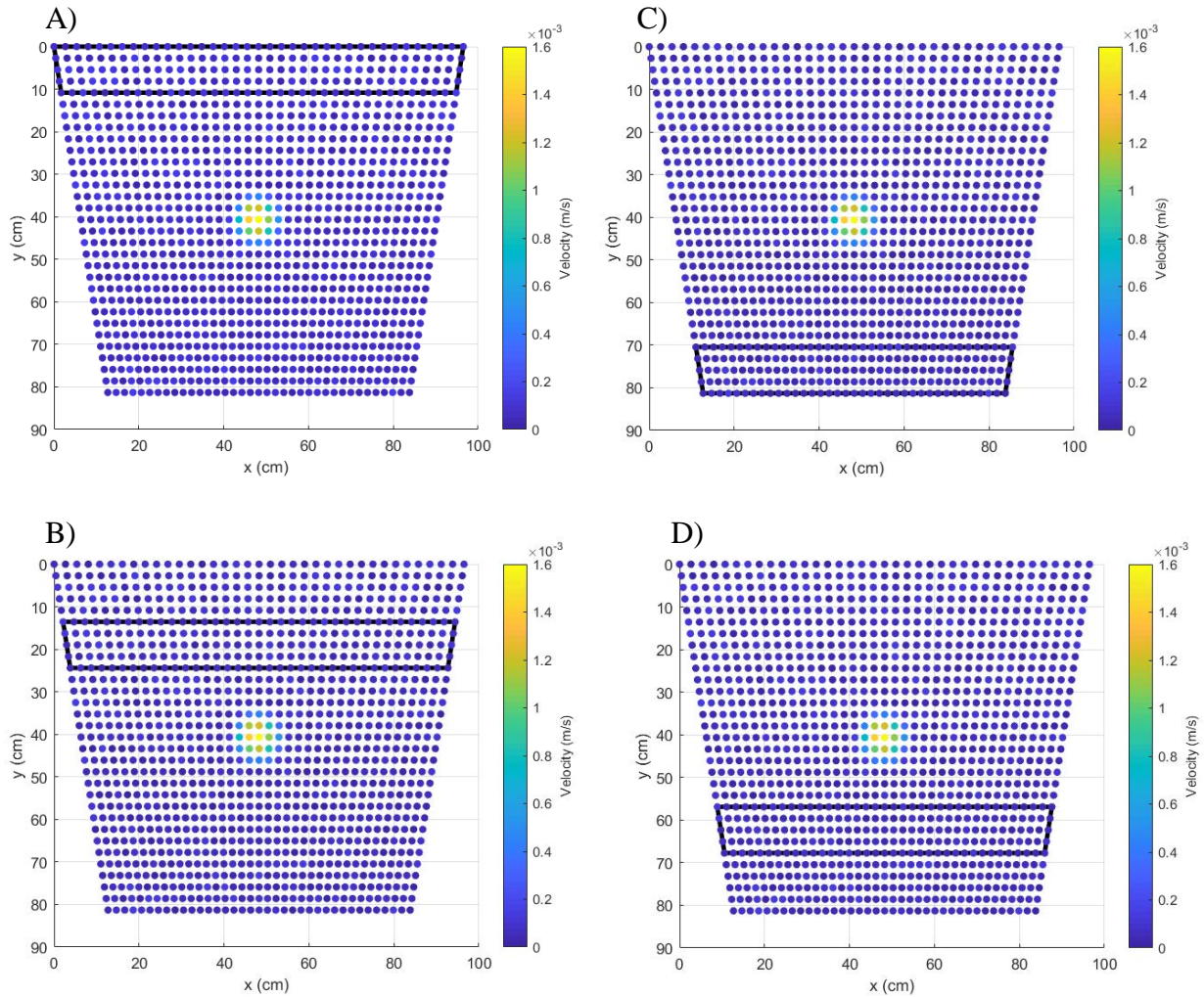
Figure 9. Velocity maps of top and bottom edges with a target. A) Top edge rows 1 to 5; B) Top edge rows 6 to 10; C) Bottom edge rows 27 to 31; D) Bottom edge rows 22 to 26.
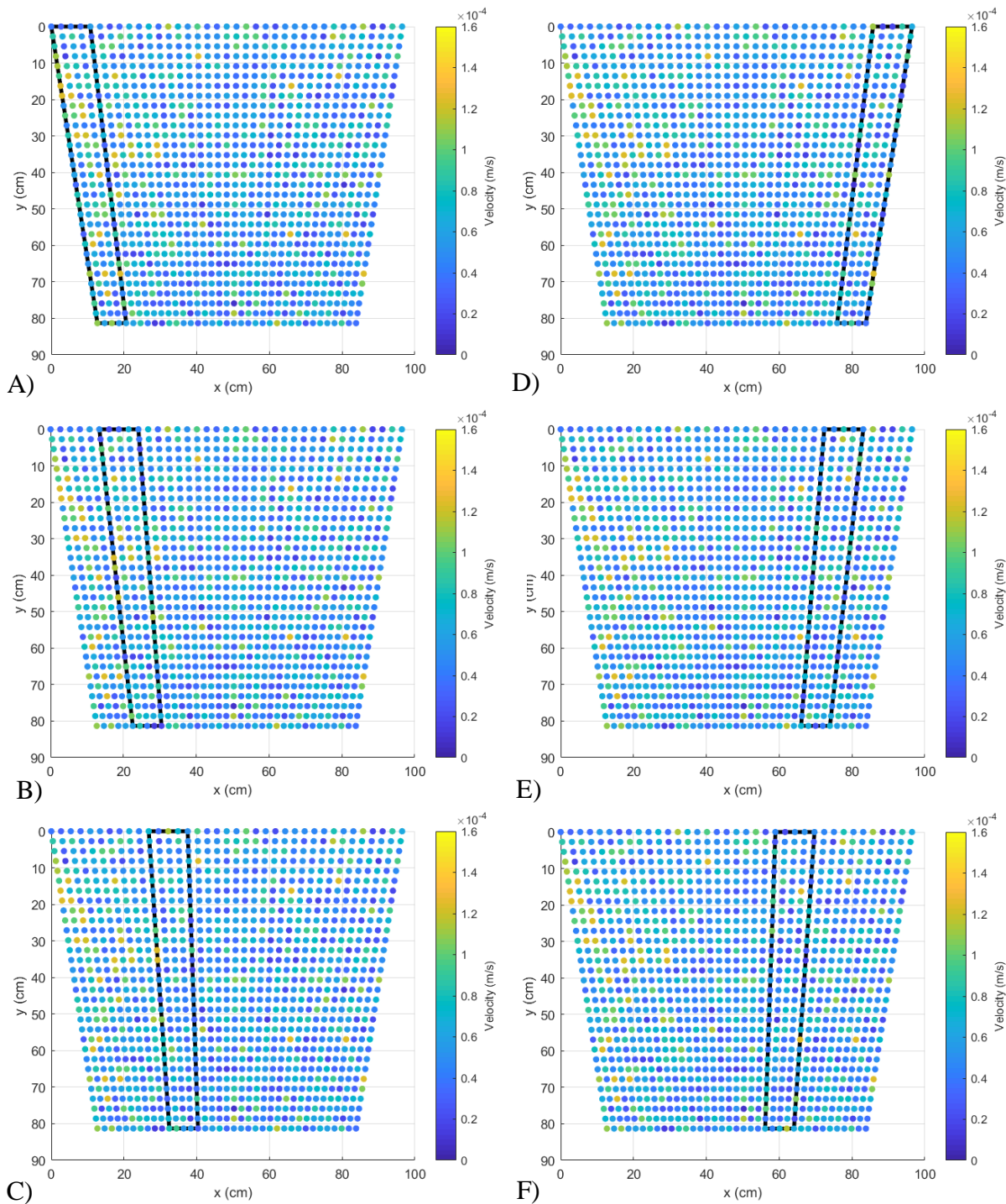
Figure 10. Velocity maps of the left and right edges of the background. A) Left edge columns 1 to 5; B) Left edge columns 6 to 10; C) Left edge columns 11 to 15. D) Right edge columns 33 to 37; E) Right edge columns 28 to 32; F) Right edge columns 23 to 27.
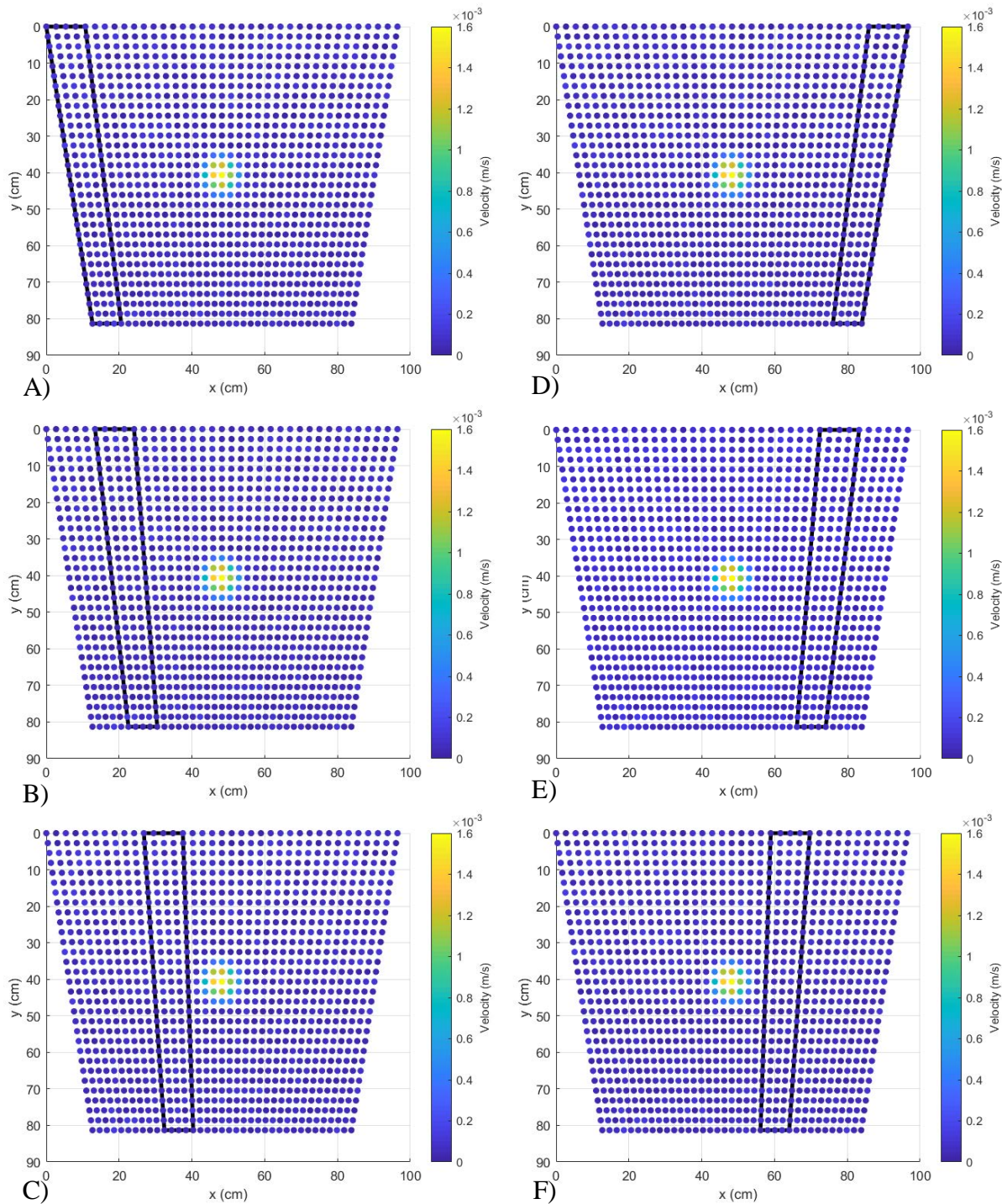
Figure 11. Velocity maps of the left and right edges with a target. A) Left edge columns 1 to 5.

B) Left edge columns 6 to 10; C) Left edge columns 11 to 15; D) Right edge columns 33 to 37.

E) Right edge columns 28 to 32; F) Right edge columns 23 to 27
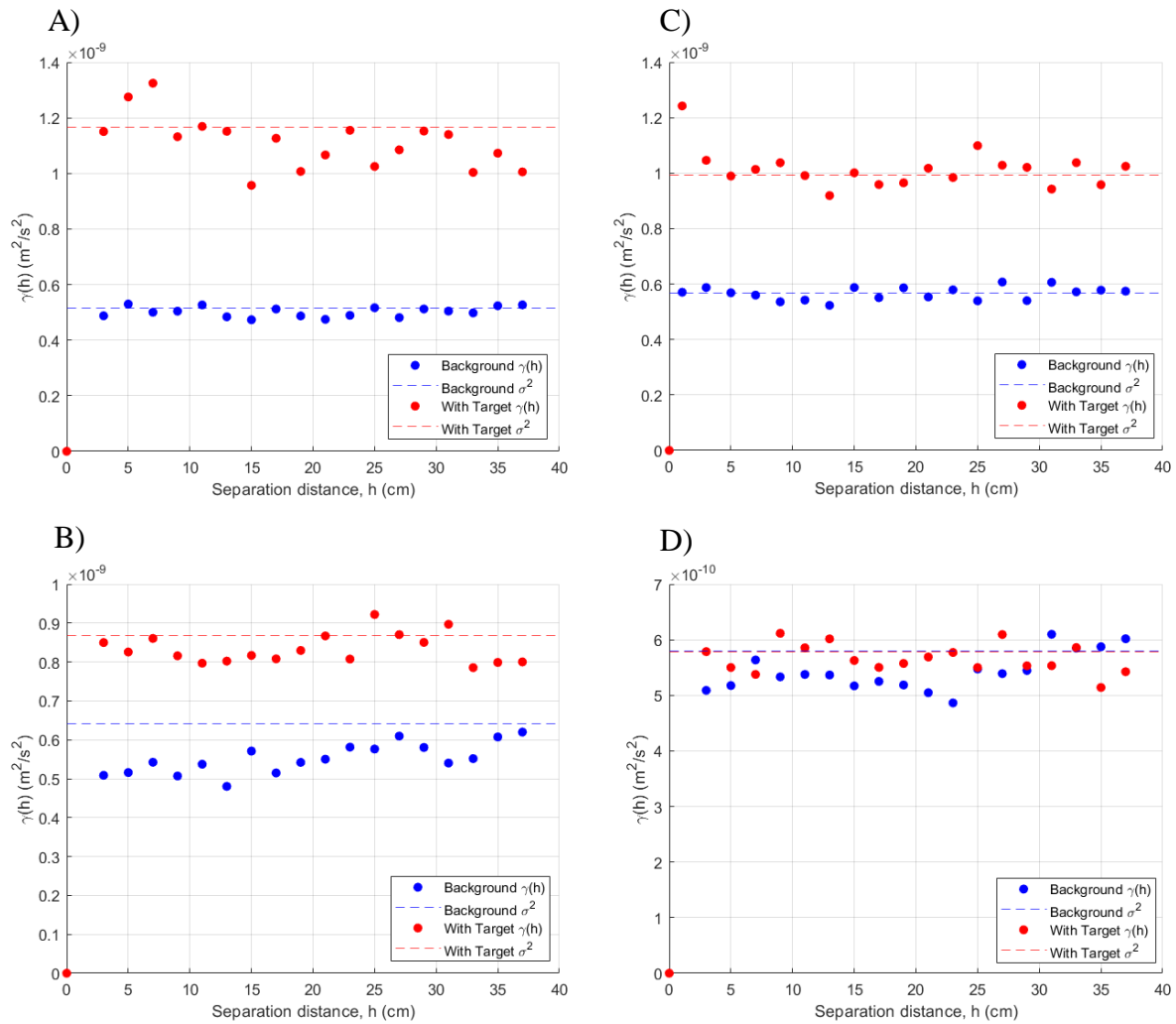
Figure 12. Variograms of top and bottom edges. A) Top edge rows 1 to 5; B) Top edge rows 6 to 10; C) Bottom edge rows 27 to 31; D) Bottom edge rows 22 to 26.
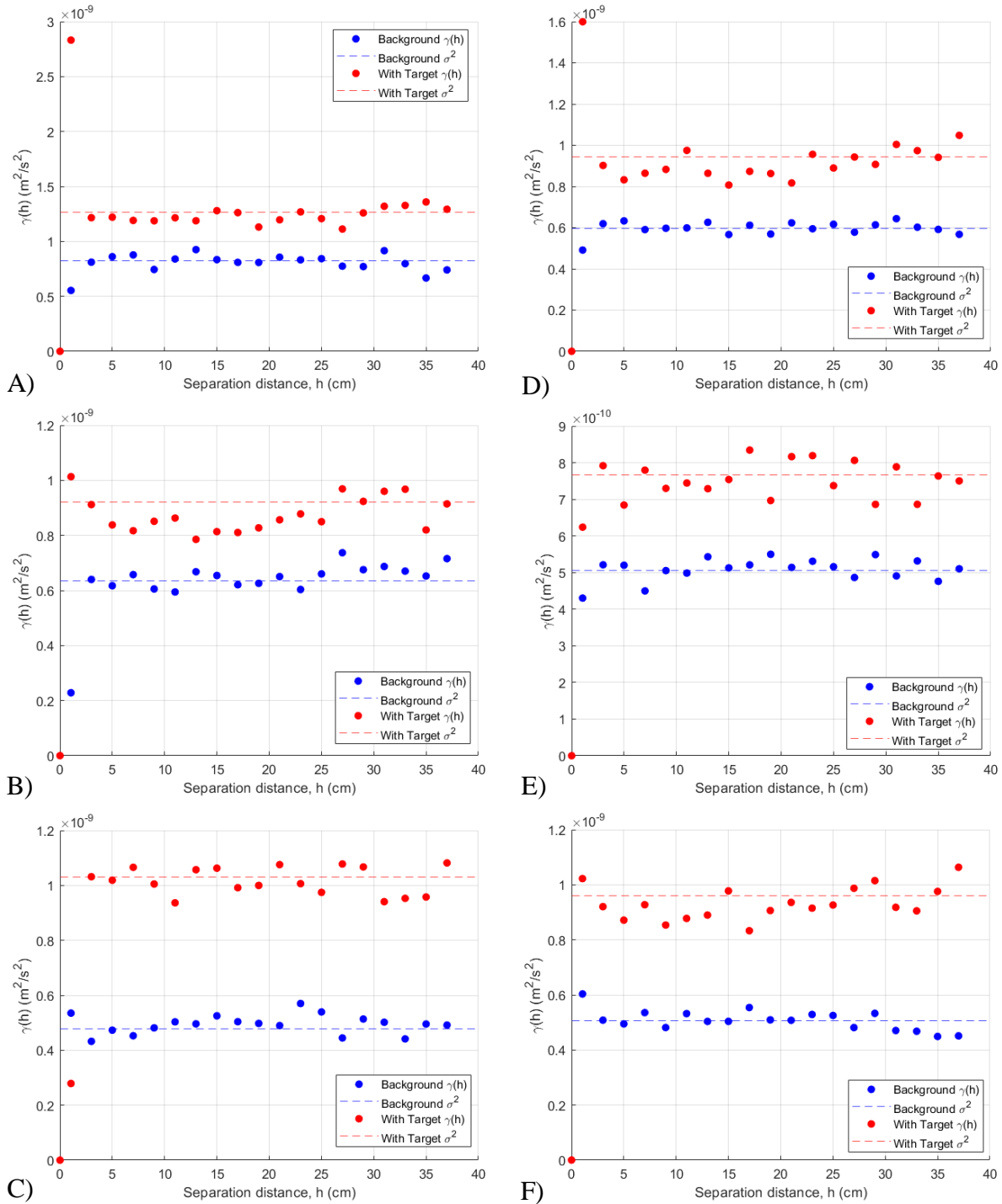
Figure 13. Variograms of the left and right edges. A) Left edge columns 1 to 5; B) Left edge columns 6 to 10; C) Left edge columns 11 to 15; D) Right edge columns 33 to 37; E) Right edge columns 28 to 32; F) Right edge columns 23 to 27.
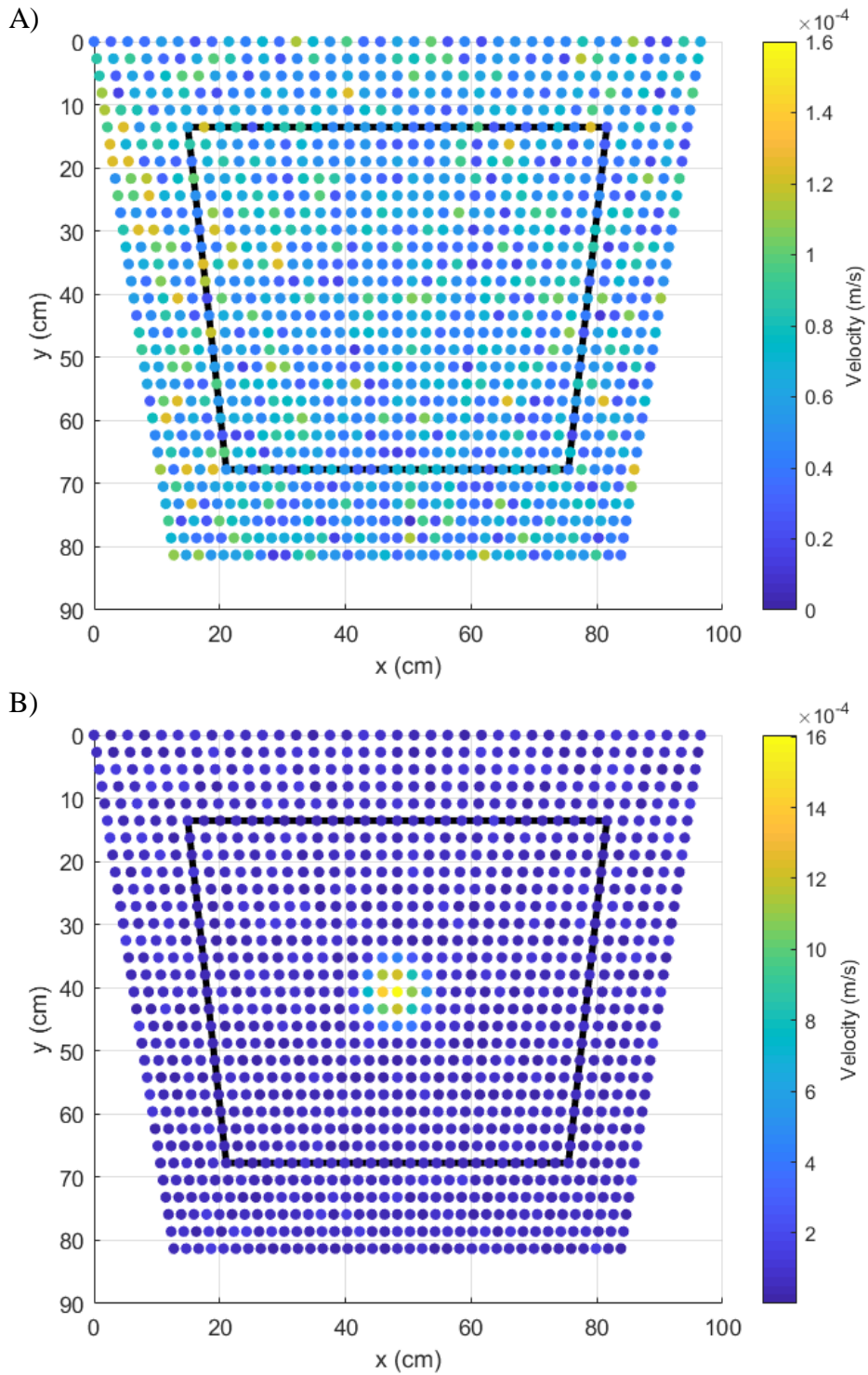
Figure 14. Map showing the reduced grid with outliers removed from both data sets. The black

shaded line represents the extent of the reduced grid. A) Background; B) With-target.

Note: Velocity scales differ to show distribution of values.
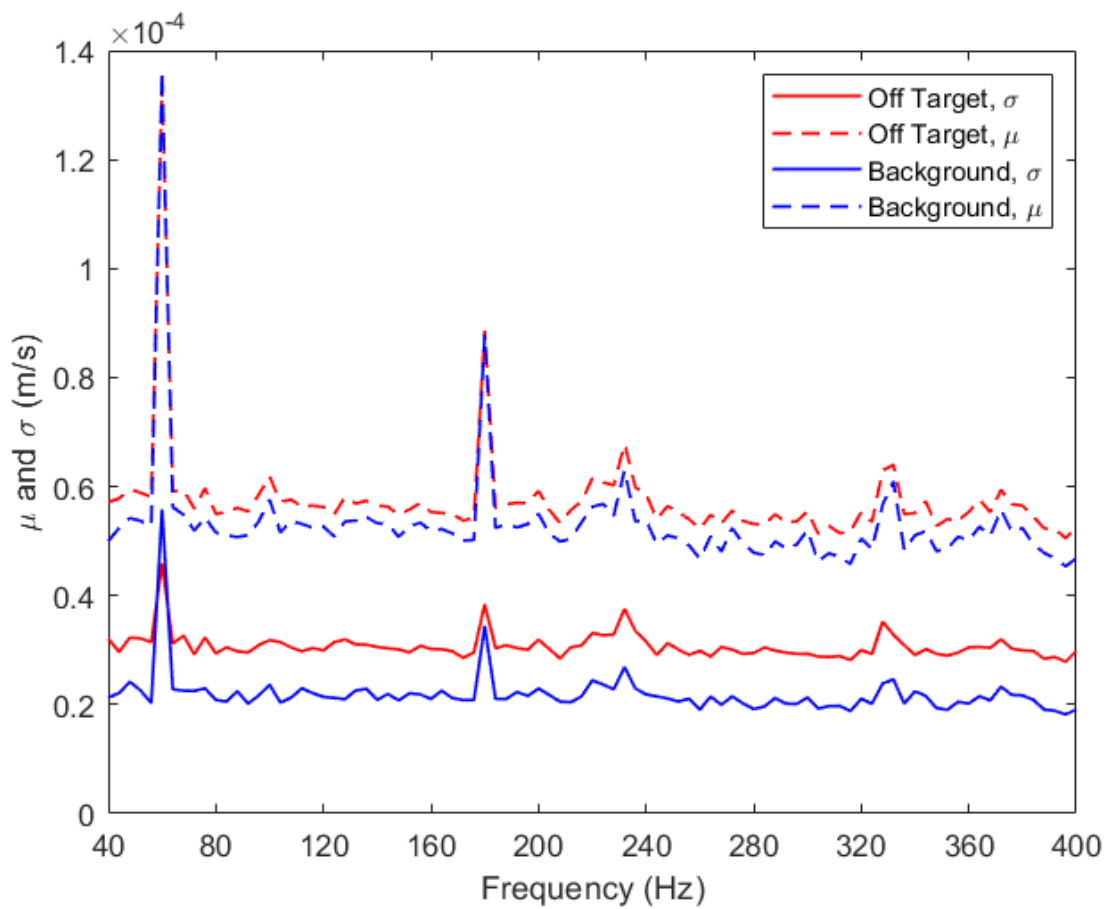
Figure 15. Mean and standard deviation as a function of frequency used in the standardization calculations. The data peaks on the plot at 60 Hz and may be associated with electrical noise. Additional peaks might be associate with resonances of the sandbox.
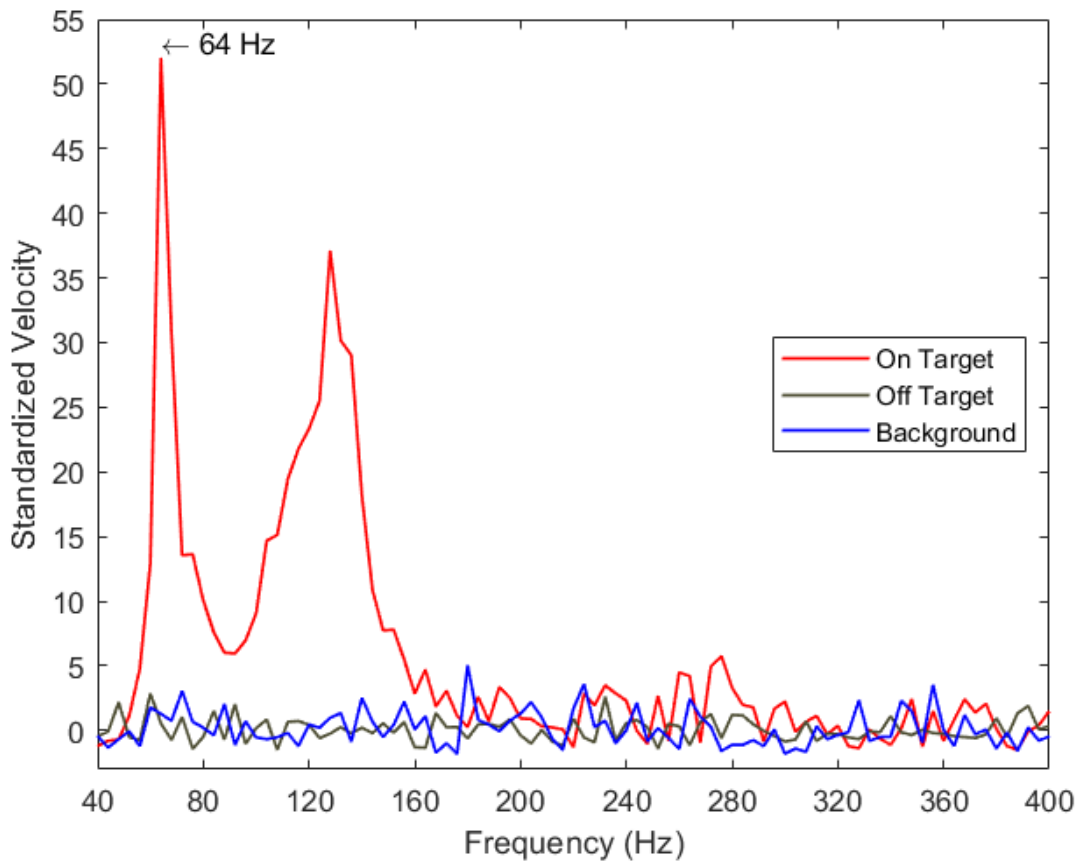
Figure 16. Spectrogram of standardized velocity on the reduced grid for points on target, off target and background velocity as a function of frequency.
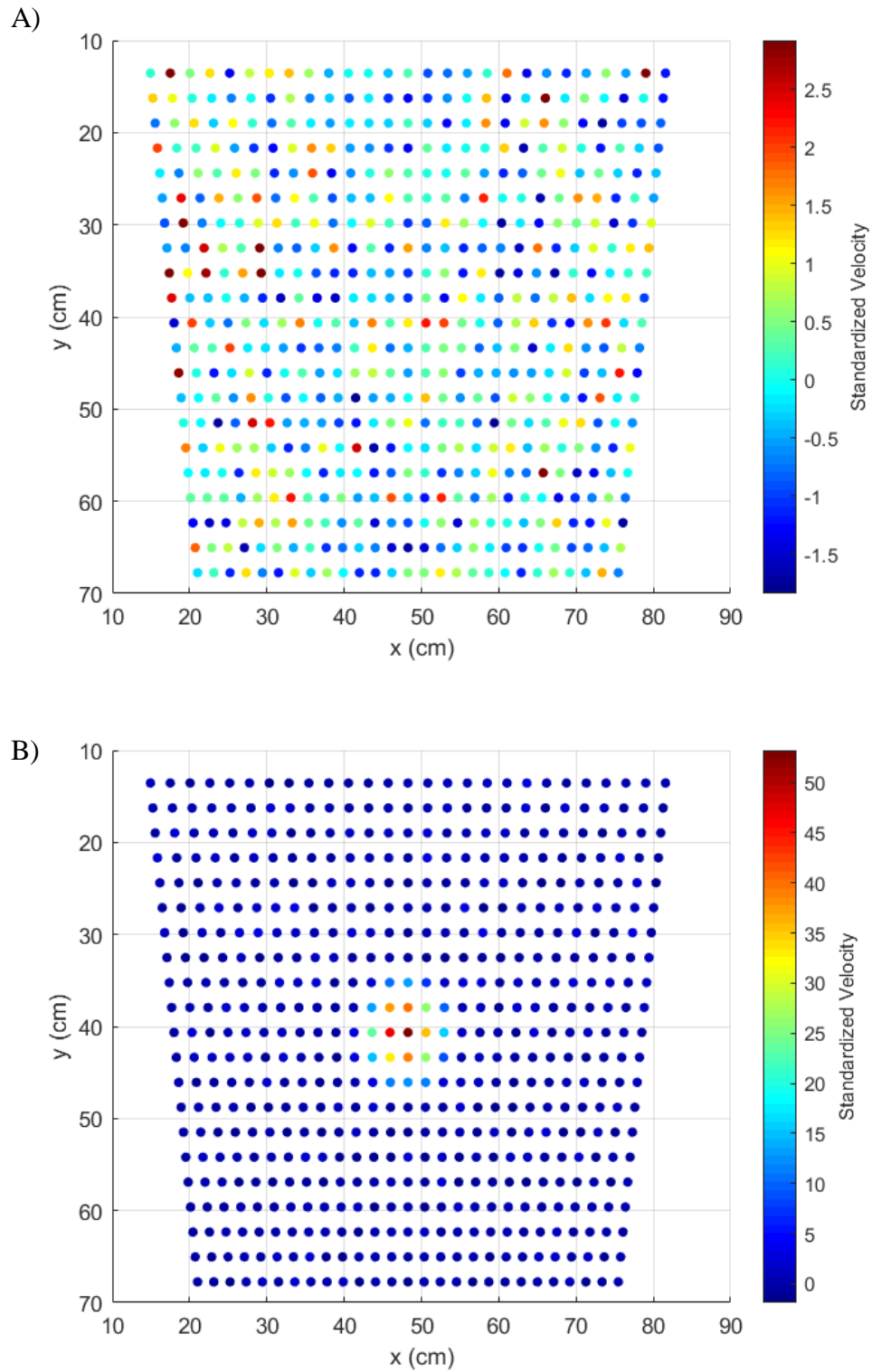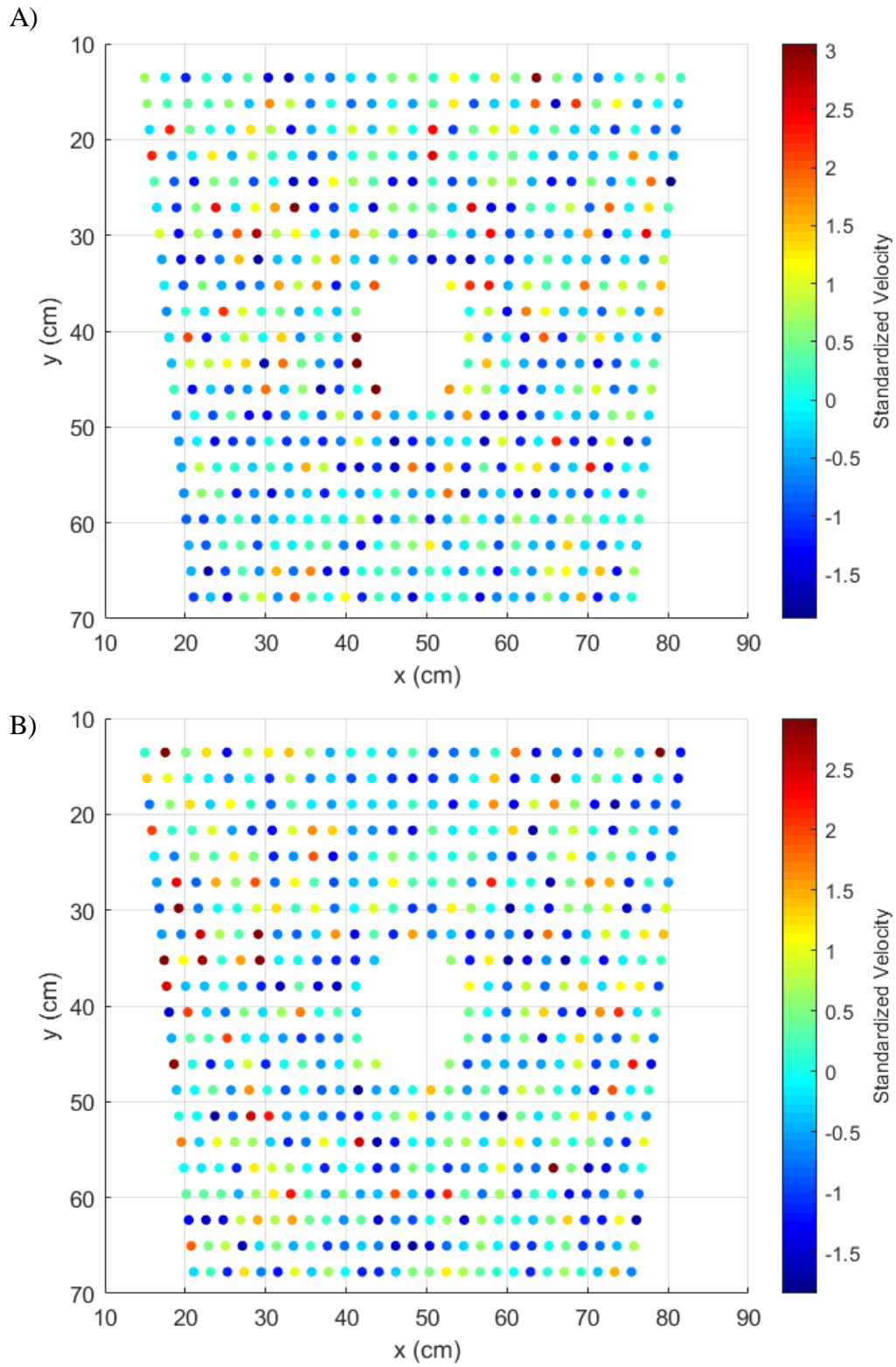
Figure 17. Standardized velocity maps. A) Background; B) With-target.

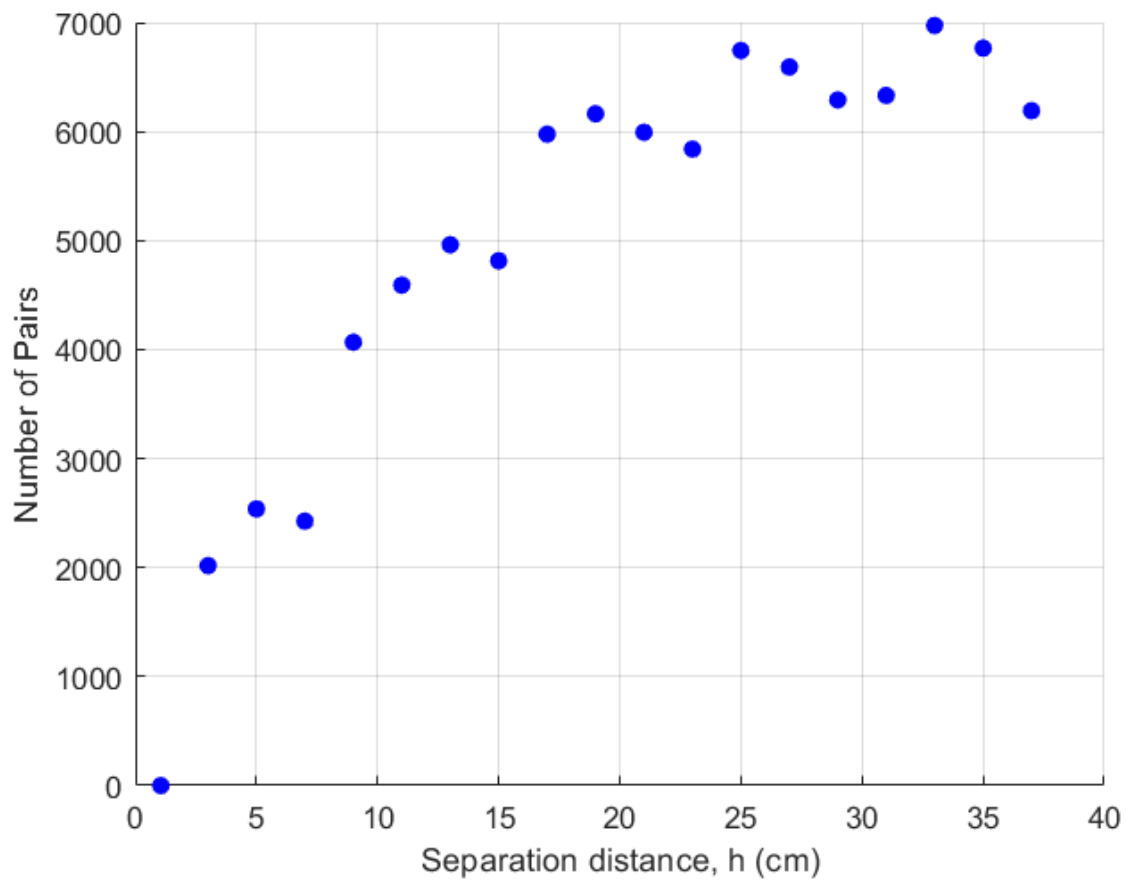Figure 18. Standardized velocity maps. A) Background; B) Off-target.

Figure 19. Number of pairs as a function of separation distance for both of the standardized
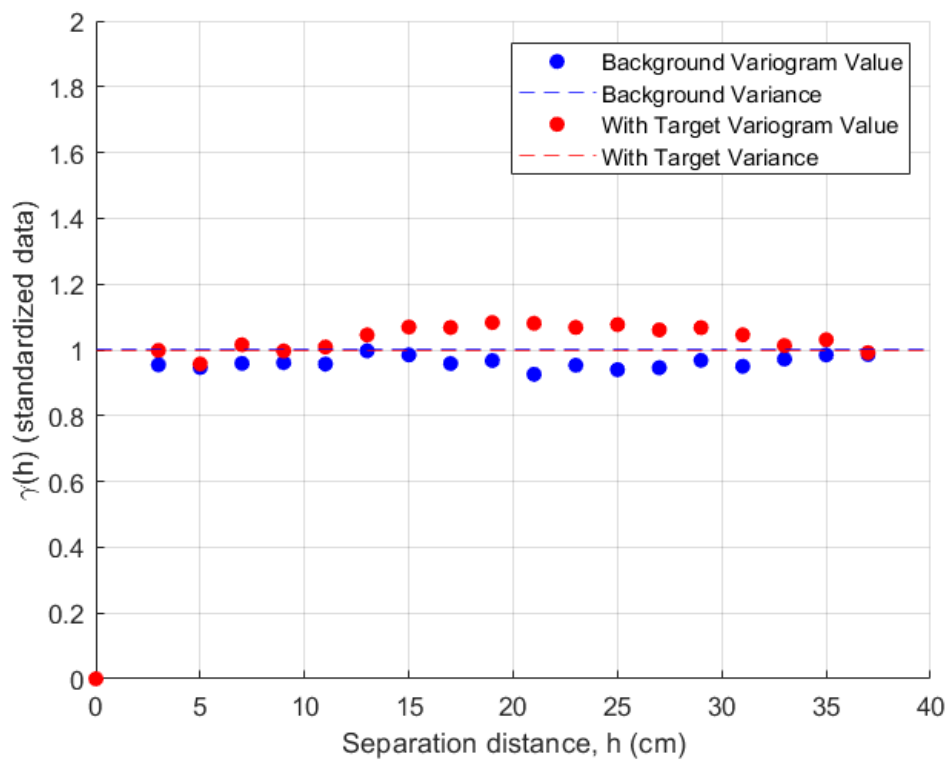
background velocity and off target velocity.

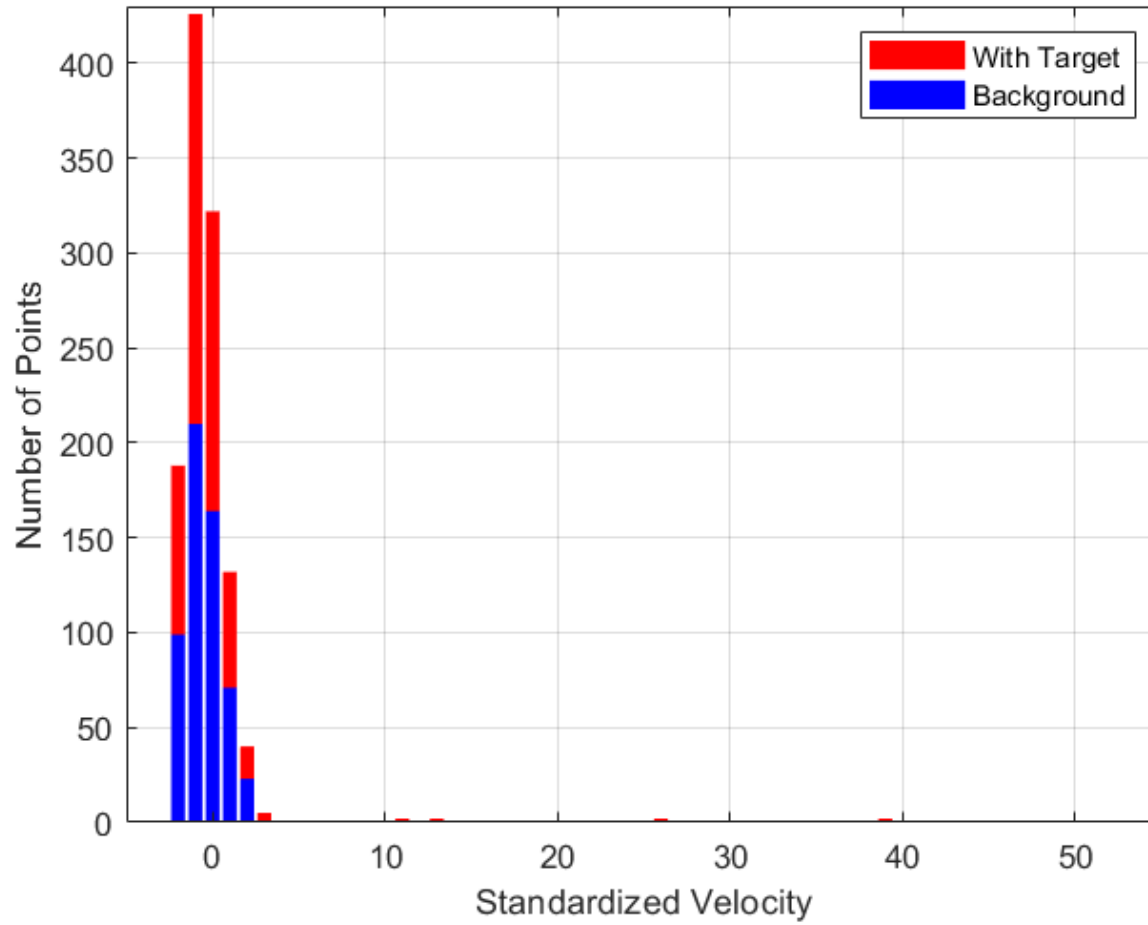Figure 20. Variogram of standardized velocity. A) Background; B) Off target.

Figure 21. Stacked histogram of standardized background velocity and velocity with a target.
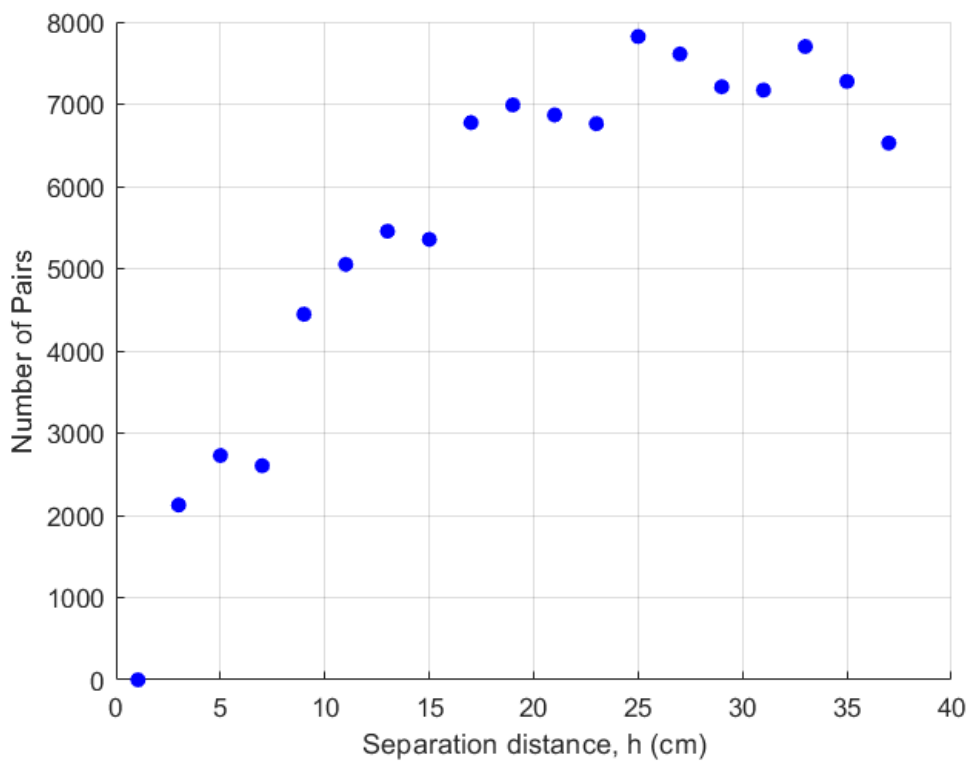
Figure 22. The number of pairs for both standardized background and buried target velocity data on a reduced grid.
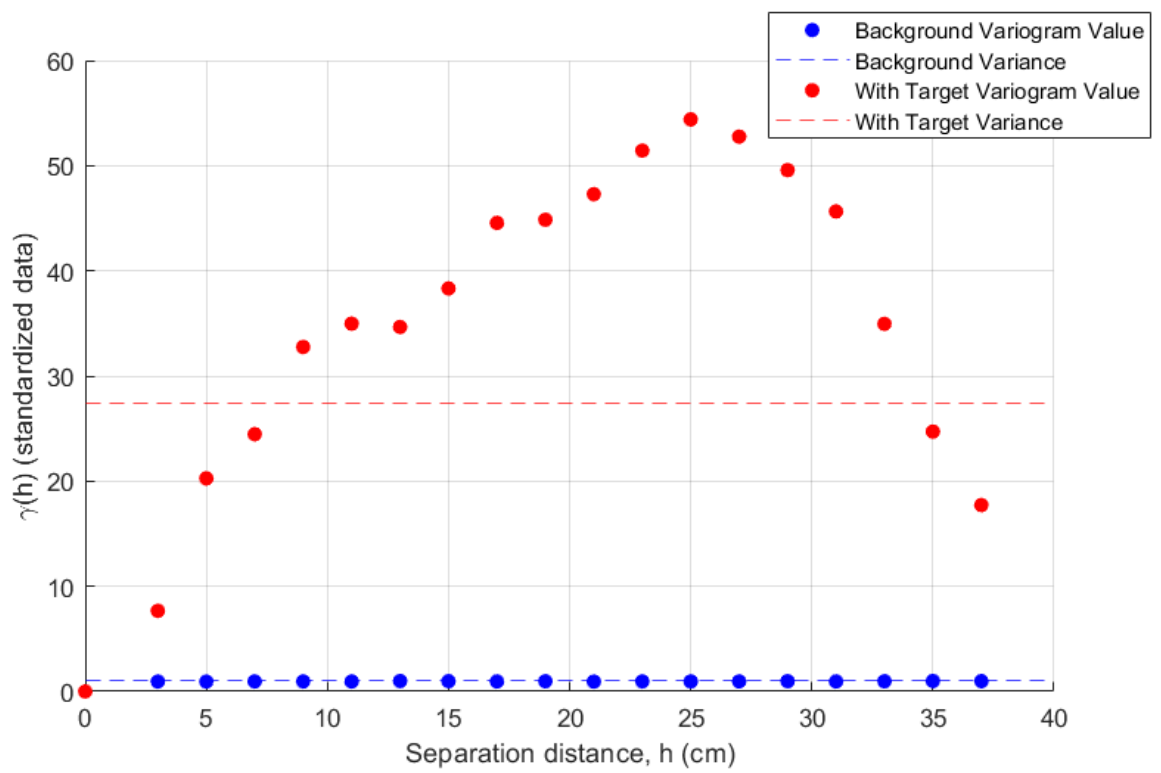
Figure 23. Variograms for standardized background velocity and standardized buried target velocity.
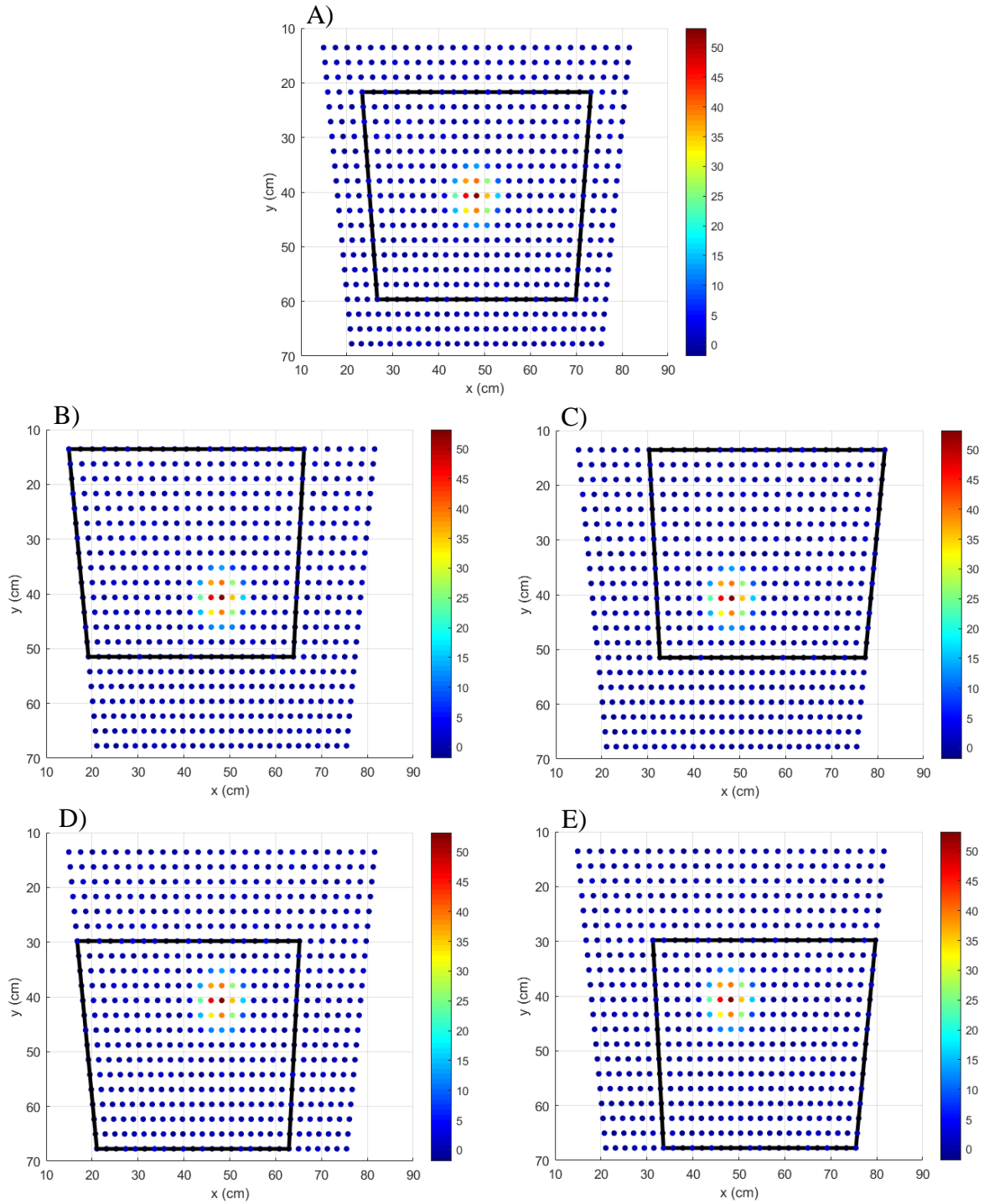
Figure 24. Velocity map of standardized target data with the frame moved in the measurement domain. A) Center of the grid; B) Top left; C) Top right; D) Bottom left; E) Bottom right.
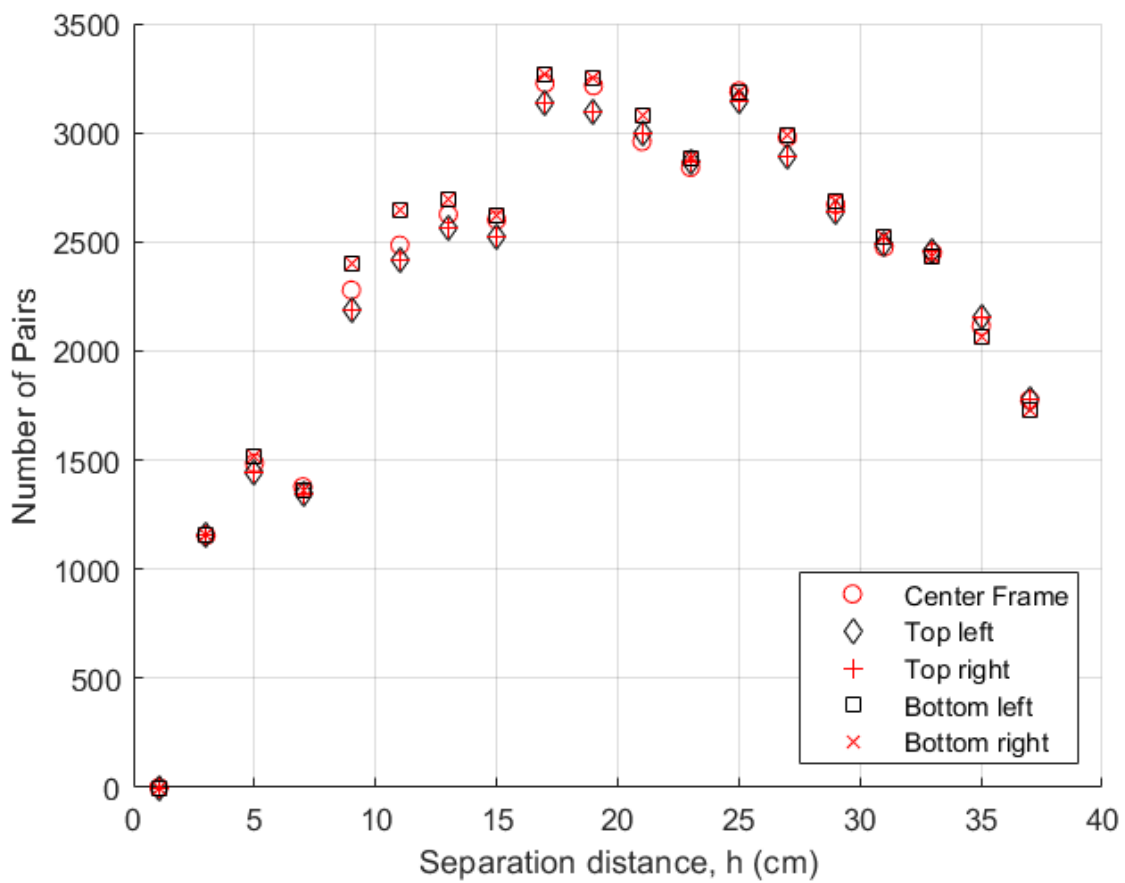
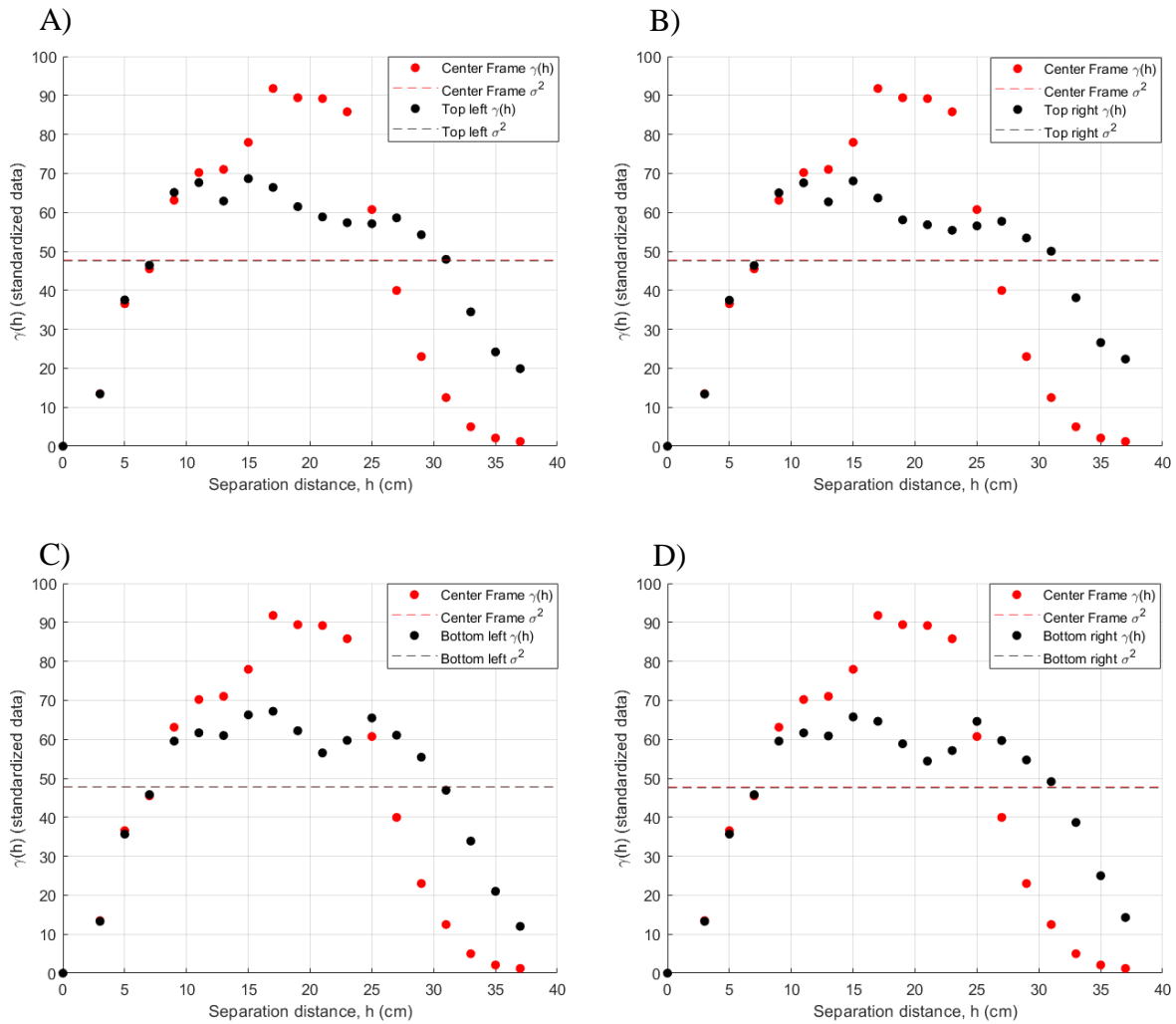Figure 25. Number of pairs for the frame moved in measurement domain.

Figure 26. Variograms for standardized target data with the frame moved in the measurement domain. A) Top left; B) Top right; C) Bottom left; D) Bottom right.
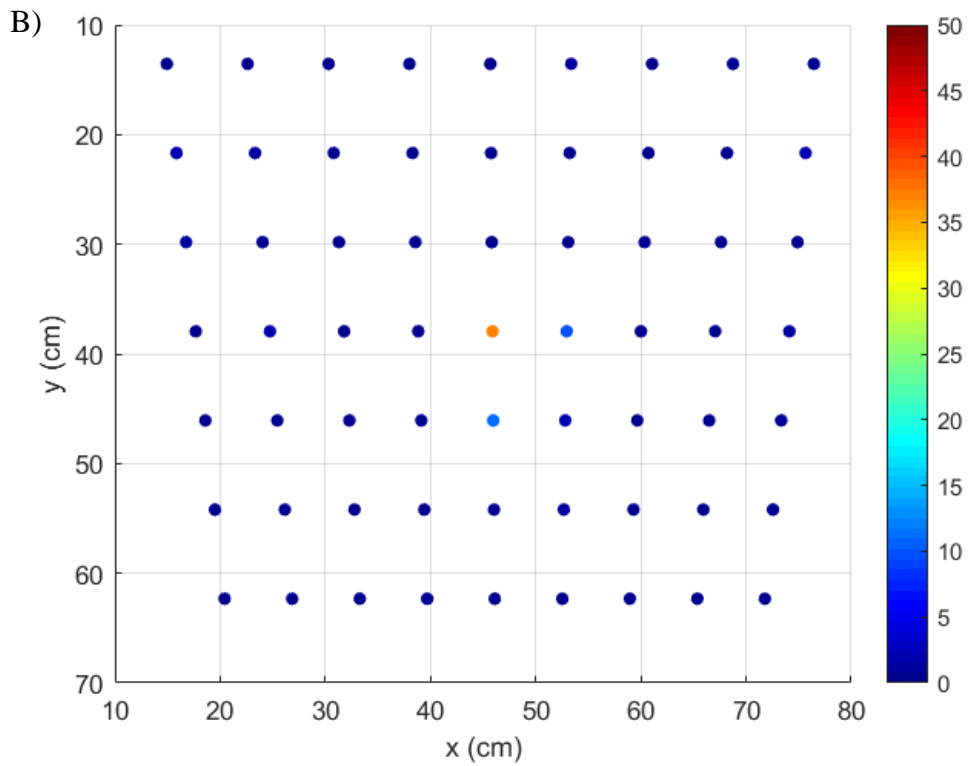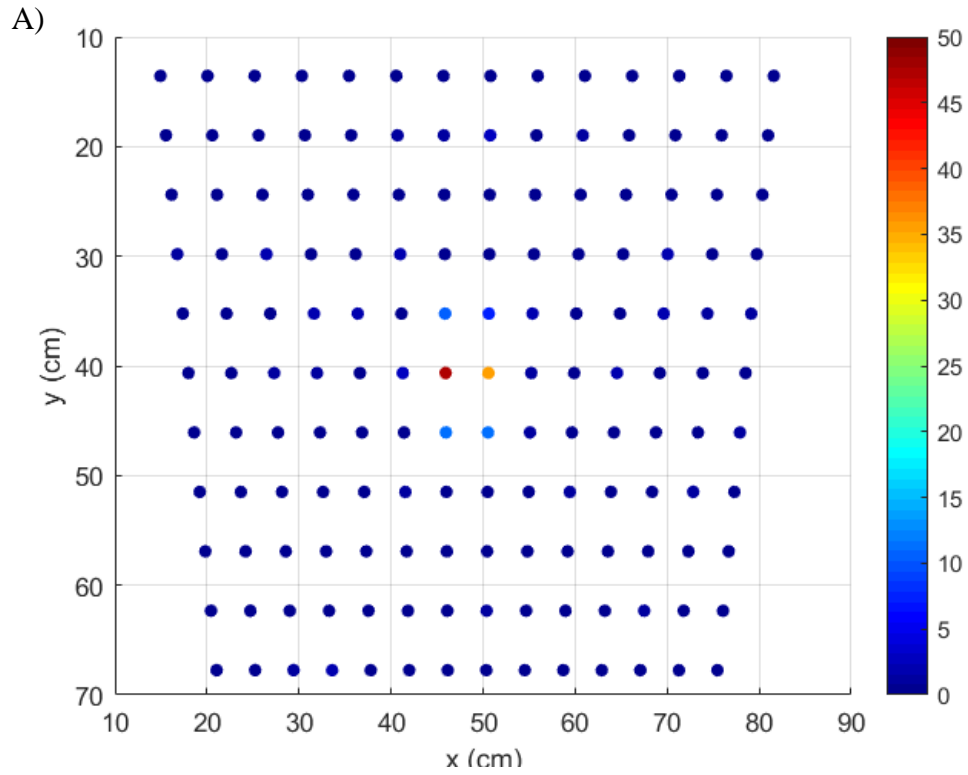
Figure 27. Velocity maps of data decimation. A) Every 2$^{nd}$ point removed; B) Every 3$^{rd}$ point removed.
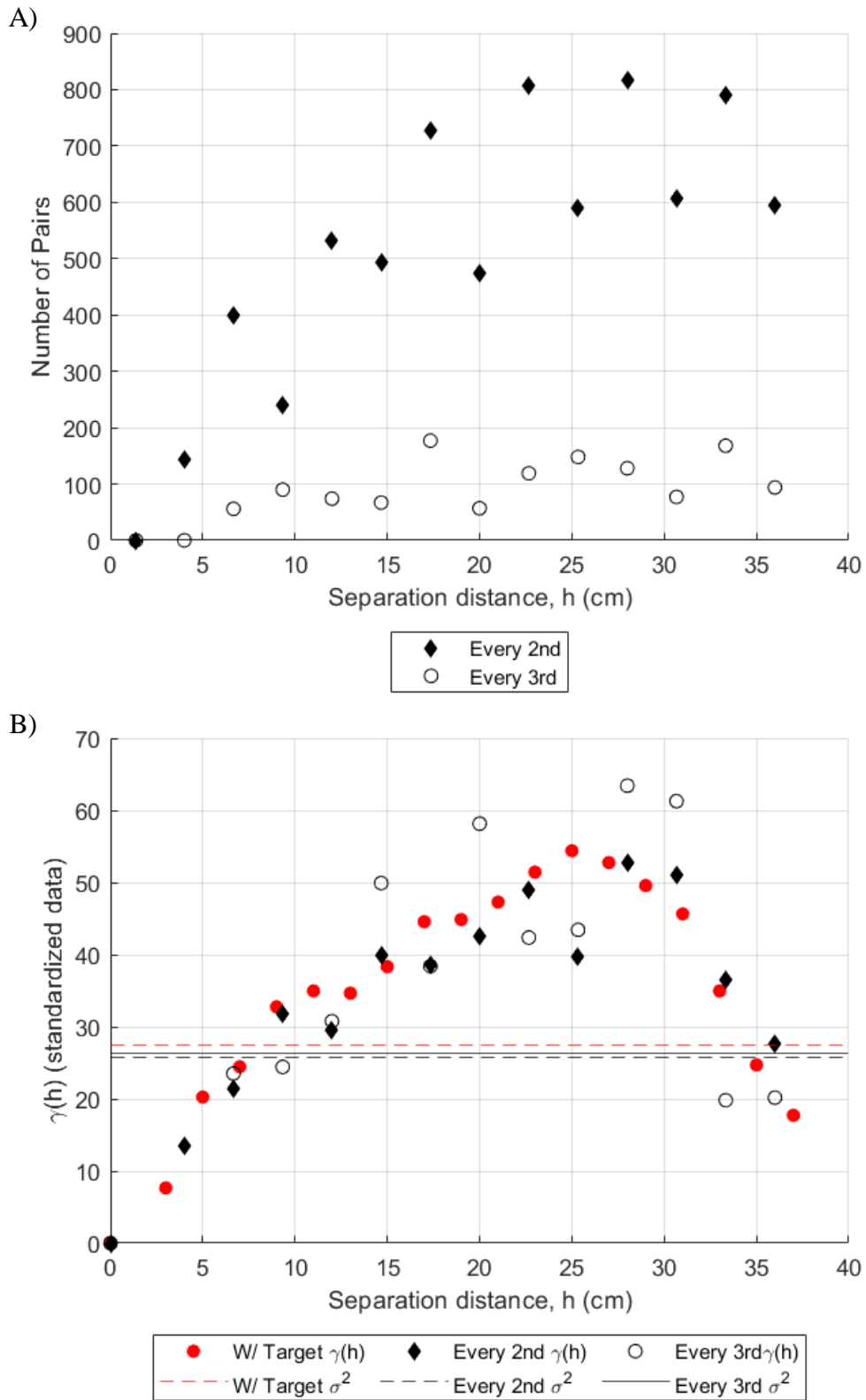
Figure 28. Data decimation. A) Number of pairs per separation distance; B) Corresponding variograms.
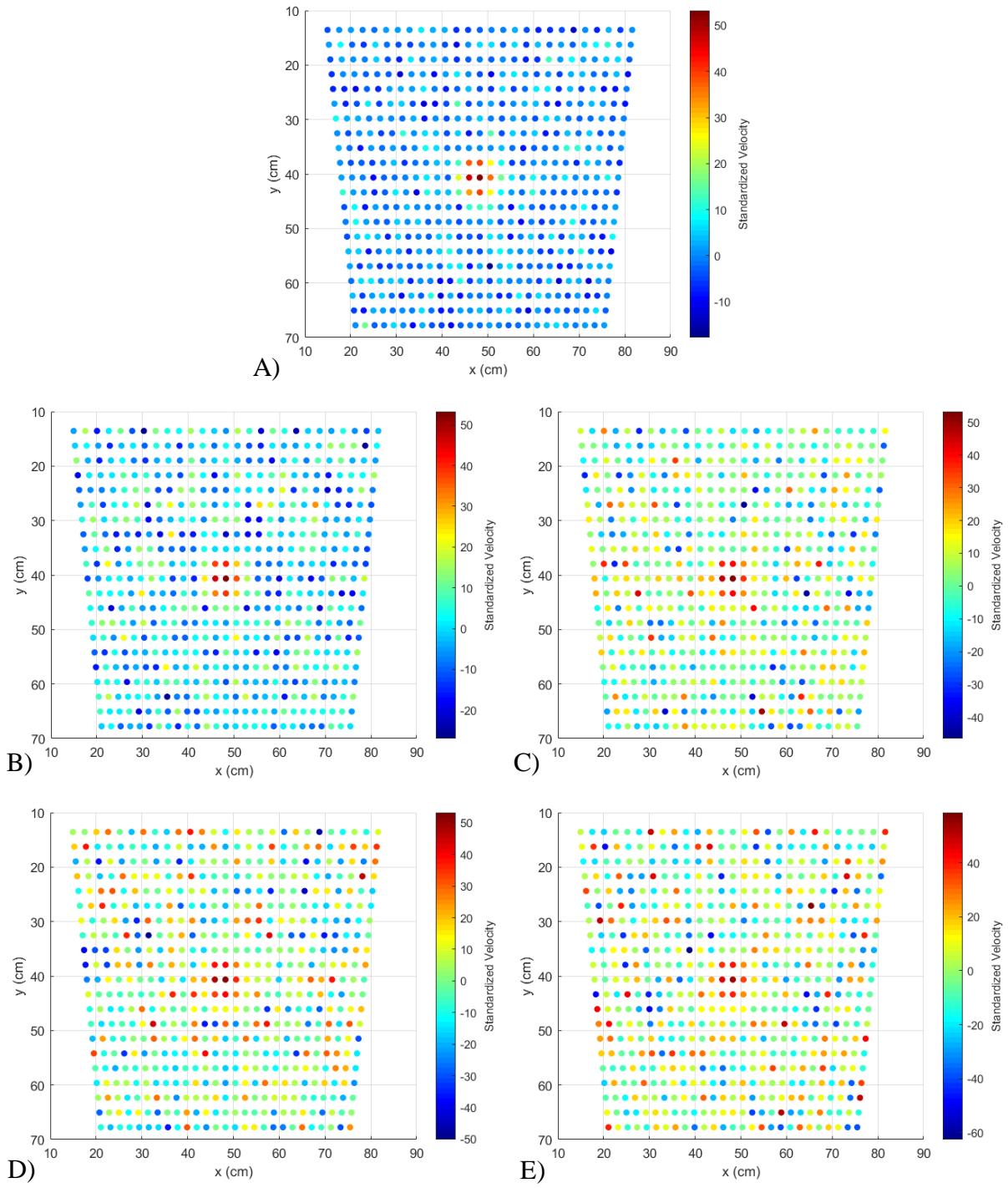
Figure 29. Velocity map of off-target observations replaced with noise having different variances

($\sigma^2$). A) $\sigma^2 = 29.7$; B) $\sigma^2 = 121$; C) $\sigma^2 = 233$; D) $\sigma^2 = 316$; D) $\sigma^2 = 438$.
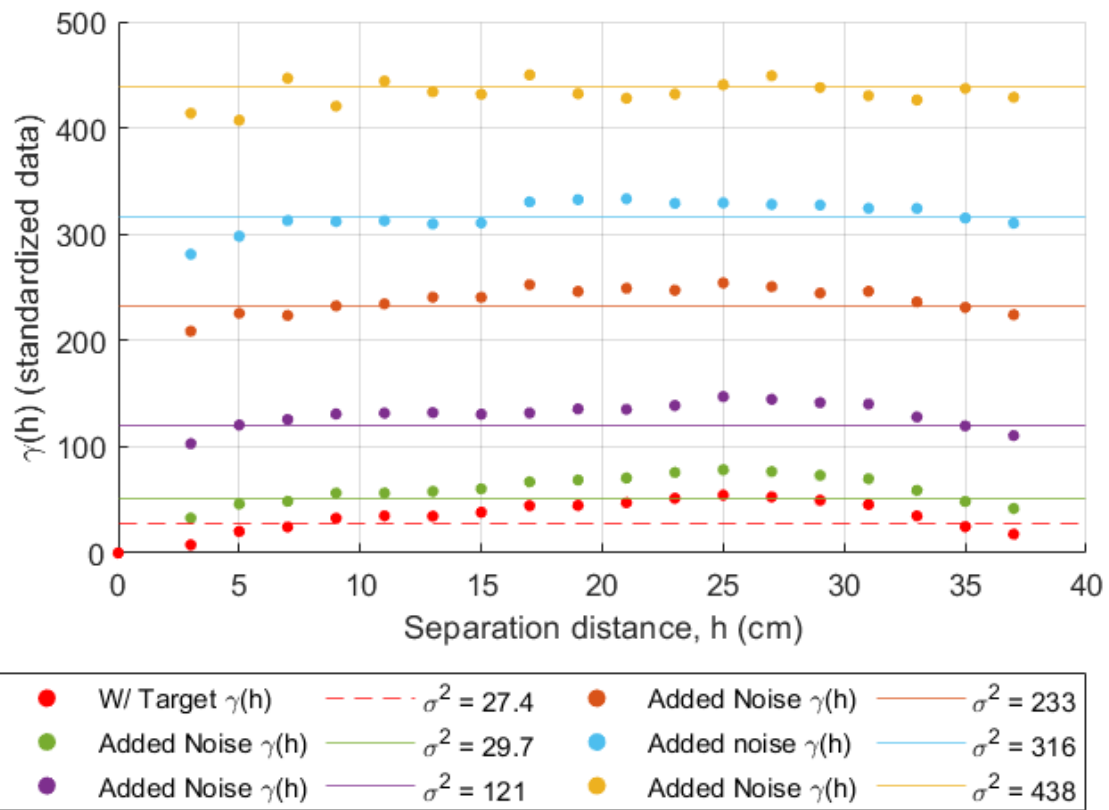
Figure 30. Added noise with increasing variances ($\sigma^2$).
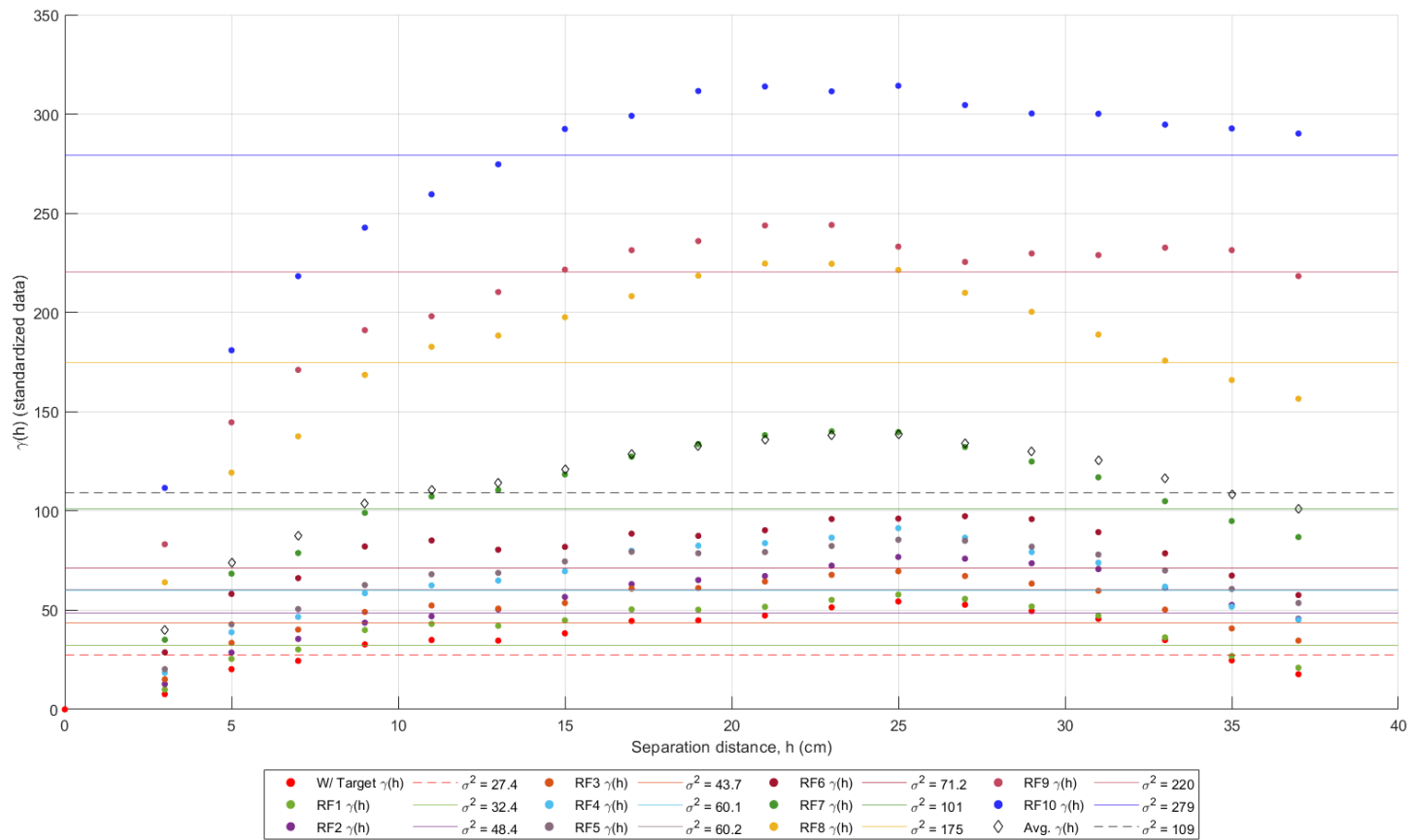
Figure 31. Variograms for off-target observations replaced with random fields (RF) of correlation lengths (λ) = 6 cm and different variances (σ²).

Figure 32. Variograms for off-target observations replaced with random fields (RF) of correlation lengths (λ) = 15 cm and different variances (σ²).
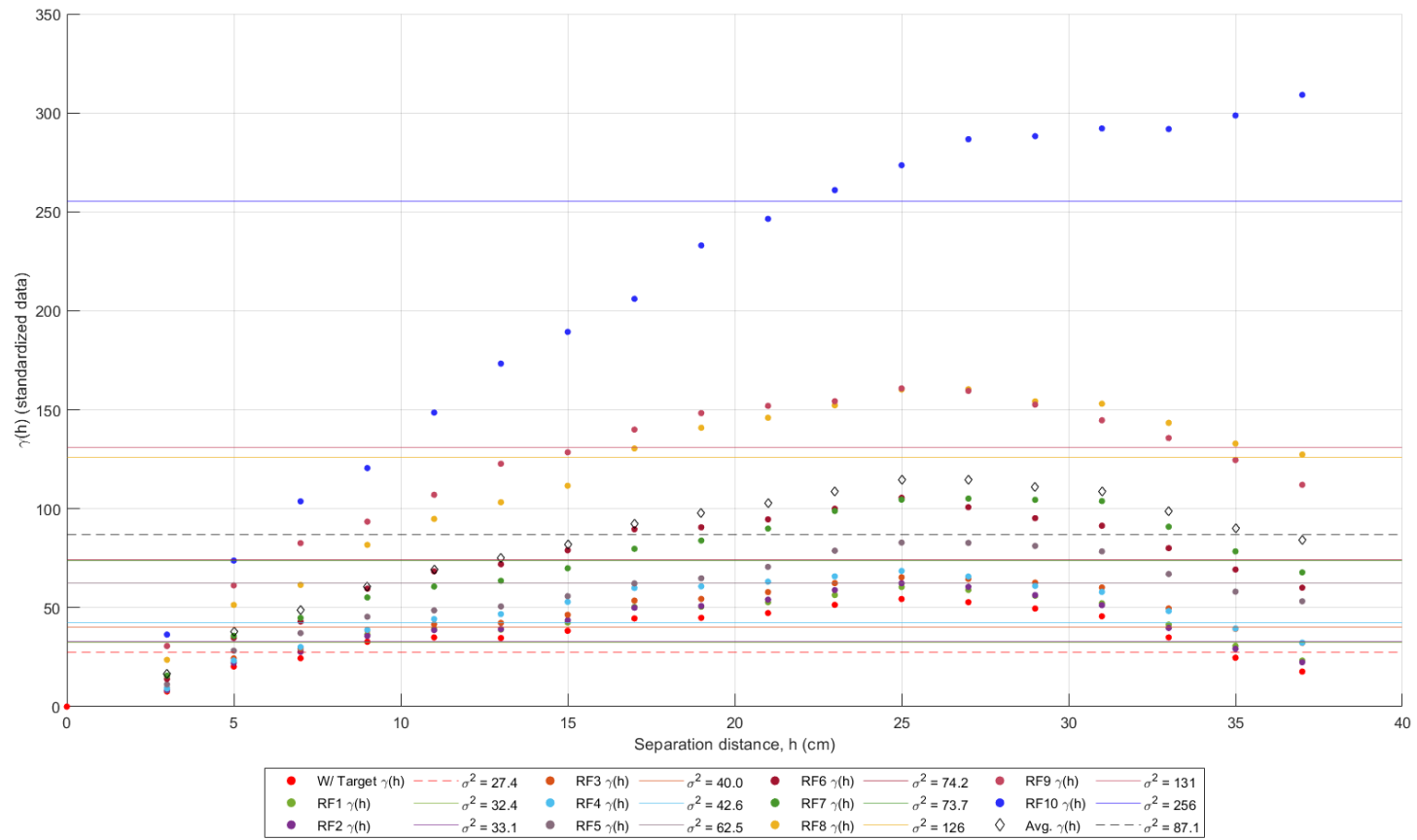
Figure 33. Variograms for off-target observations replaced with random fields (RF) of correlation lengths (λ) = 30 cm and different variances (σ²).
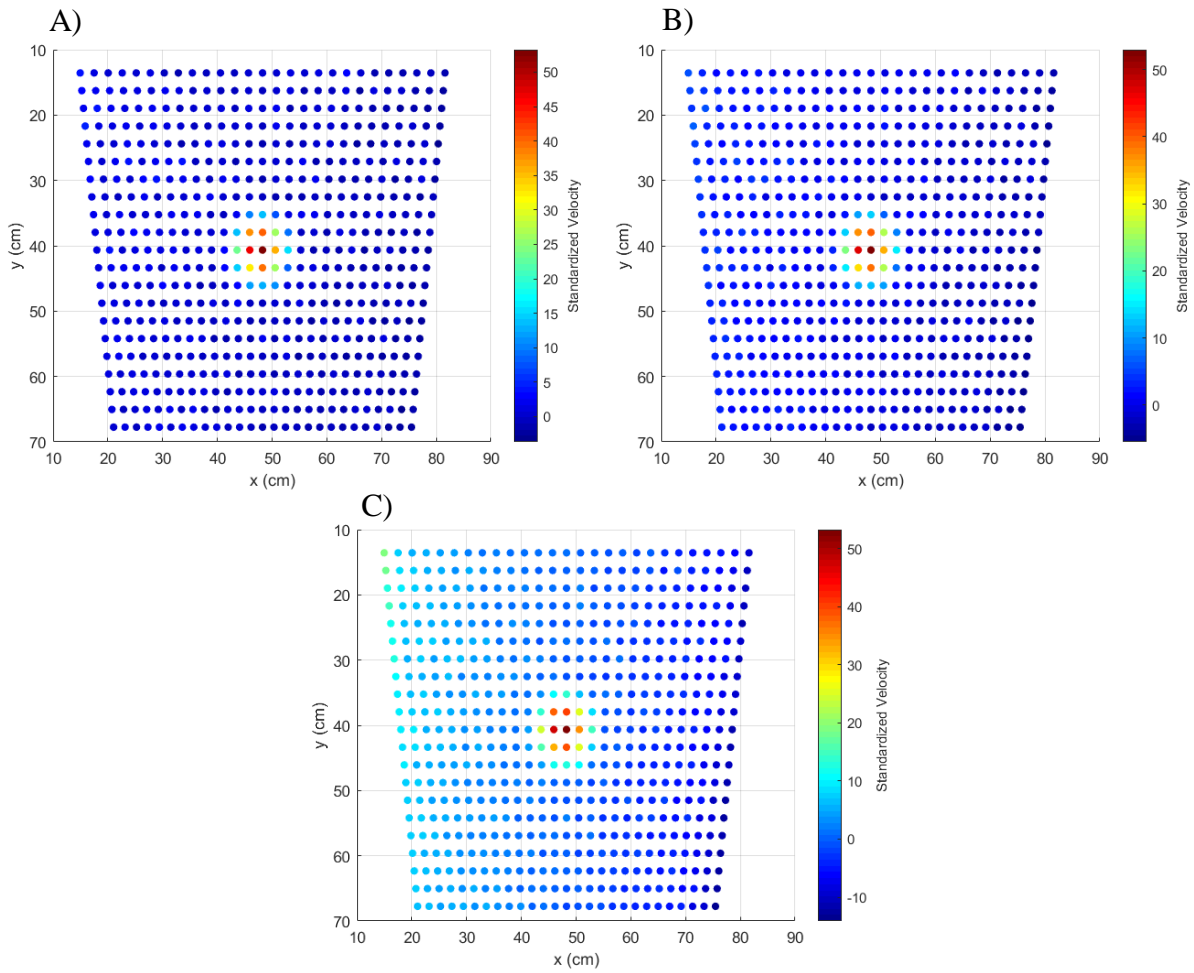
Figure 34. Velocity maps of data with added trends using different variances ($\sigma^2$). A) $\sigma^2 = 27.3$; B) $\sigma^2 = 31.2$; C) $\sigma^2 = 50.7$.
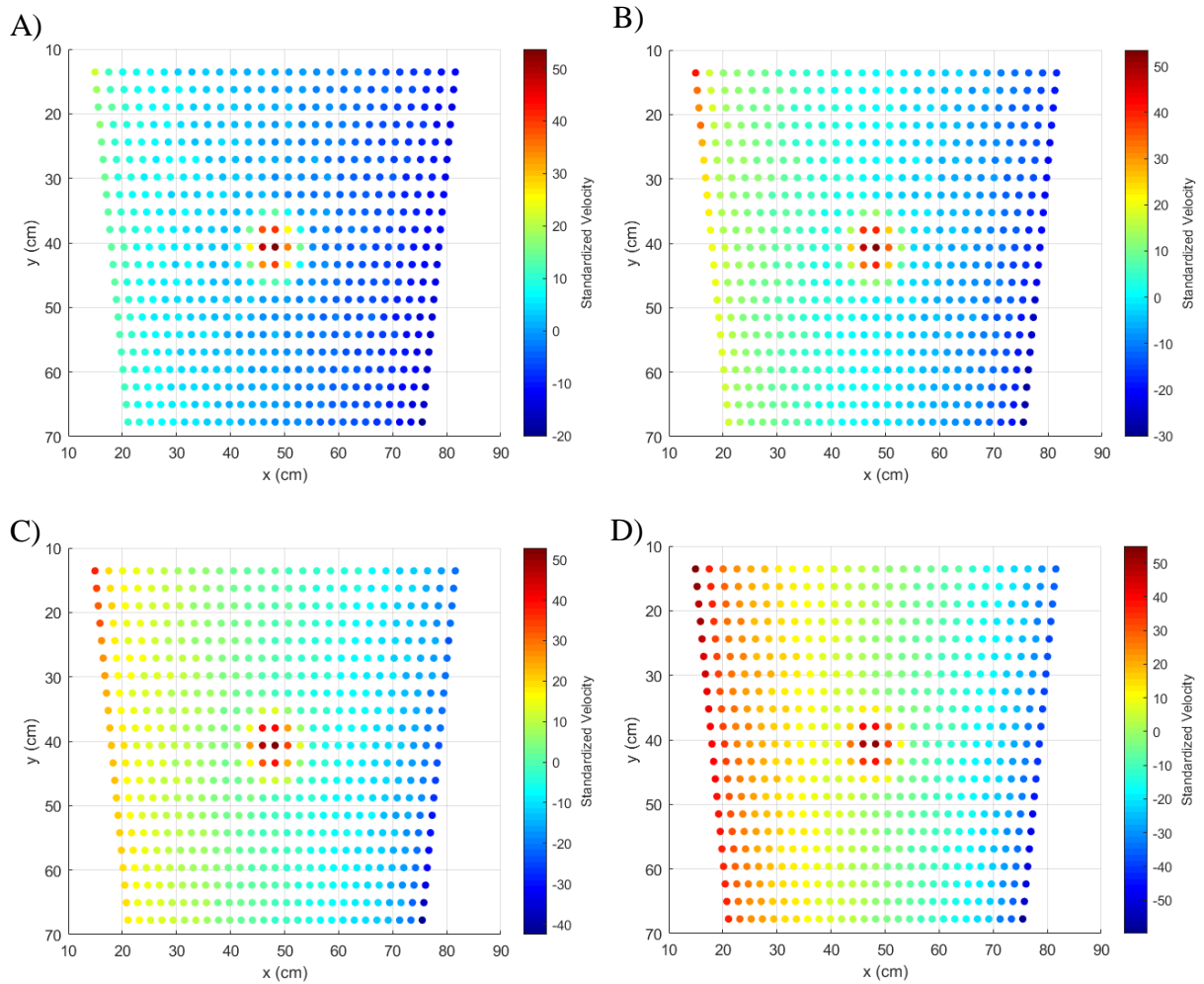
Figure 35. Velocity maps of data with added trends using different variances ($\sigma^2$). A) $\sigma^2 = 72.9$; B) $\sigma^2 = 130$; C) $\sigma^2 = 165$; D) $\sigma^2 = 417$.
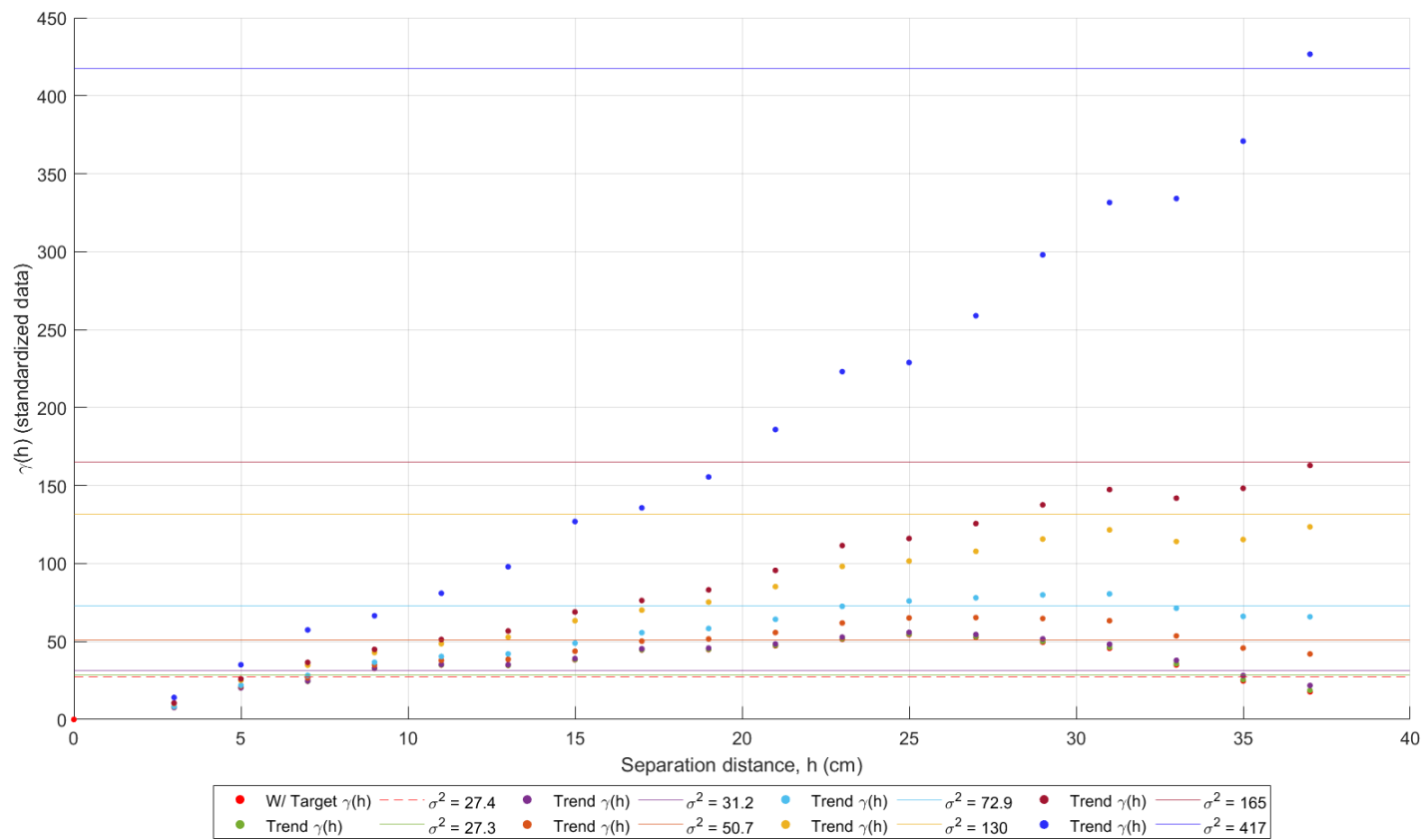
Figure 36. Variograms of data with added trend calculated at different variances ($\sigma^2$).
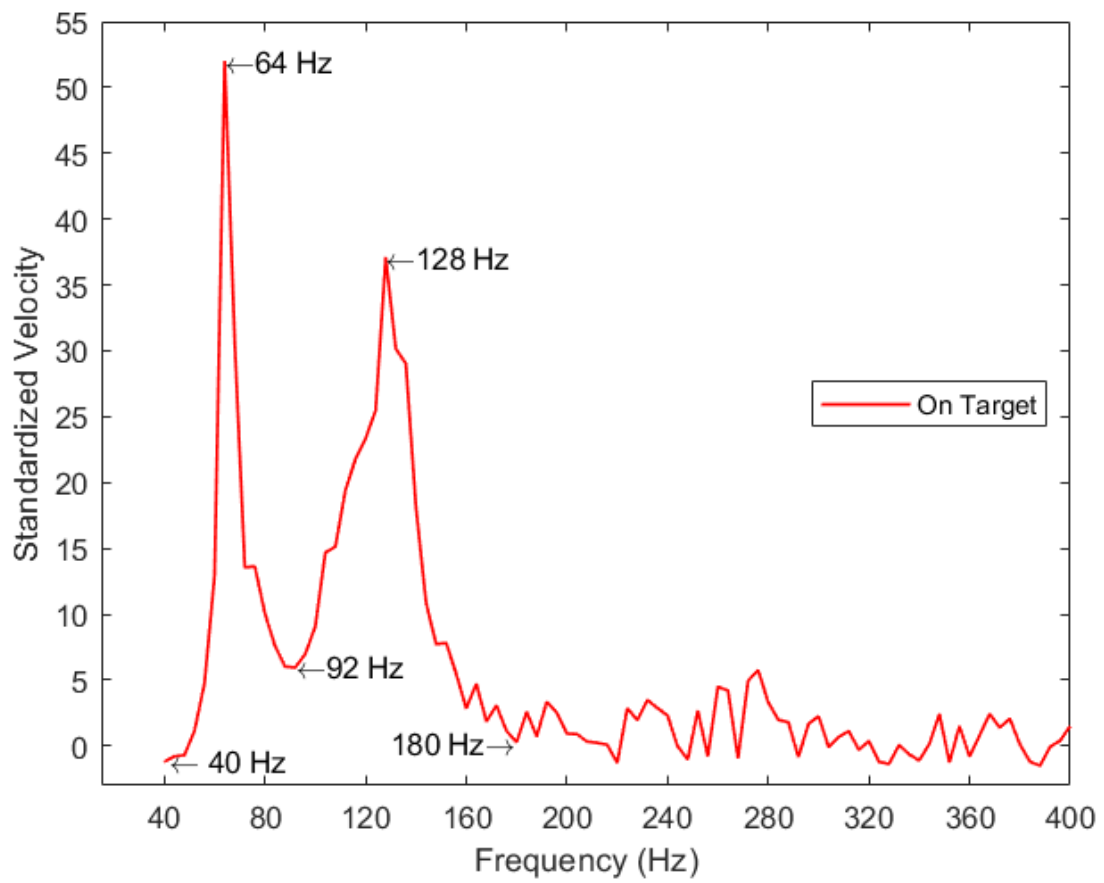
Figure 37. Spectrogram of peaks and throughs on target.

A)



B)
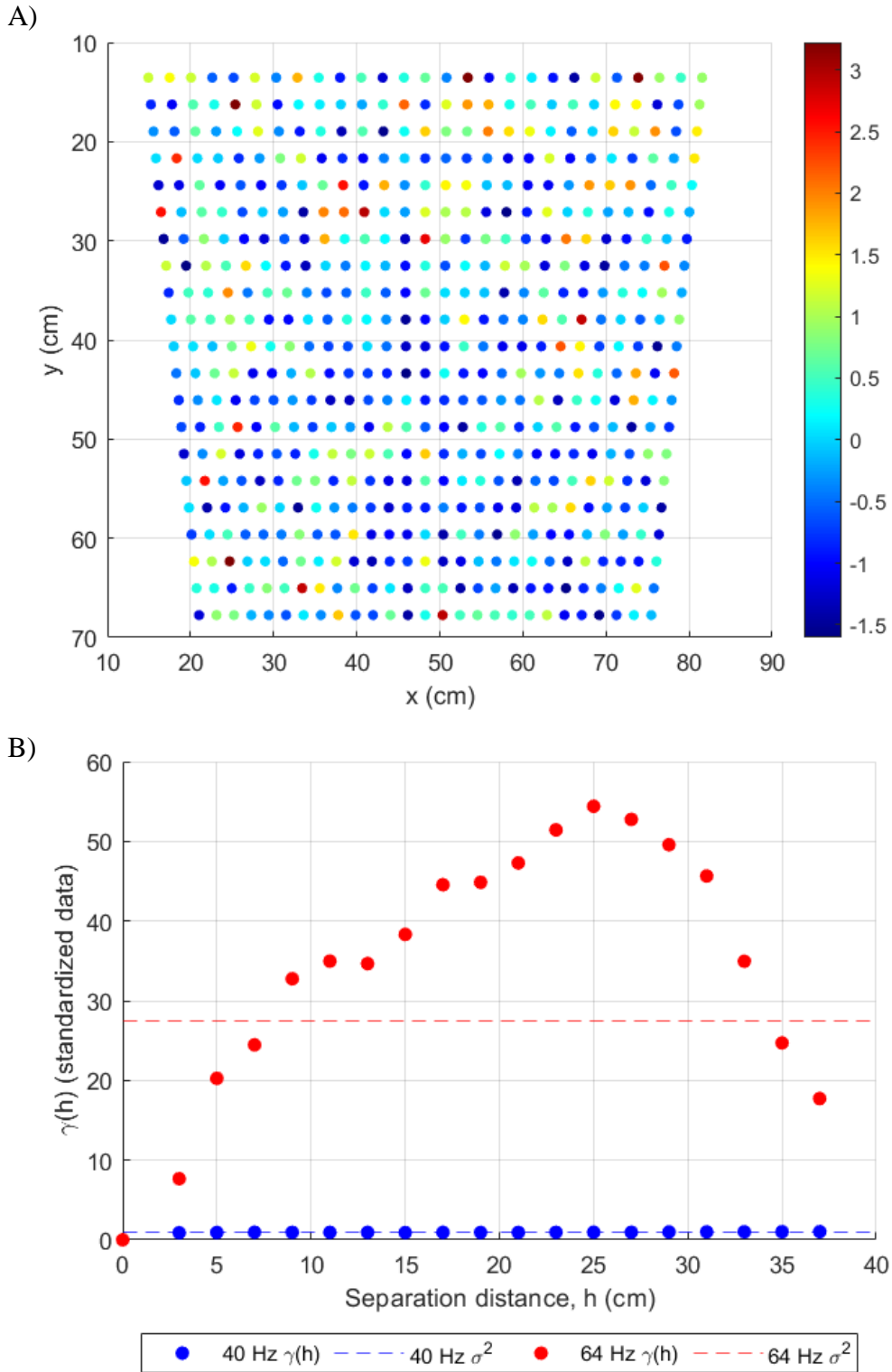


Figure 38. Velocity map and variogram of standardized and reduced velocity of target data at 40 Hz. A) Velocity map at 40 Hz; B) Variogram at 40 Hz and 64 Hz.
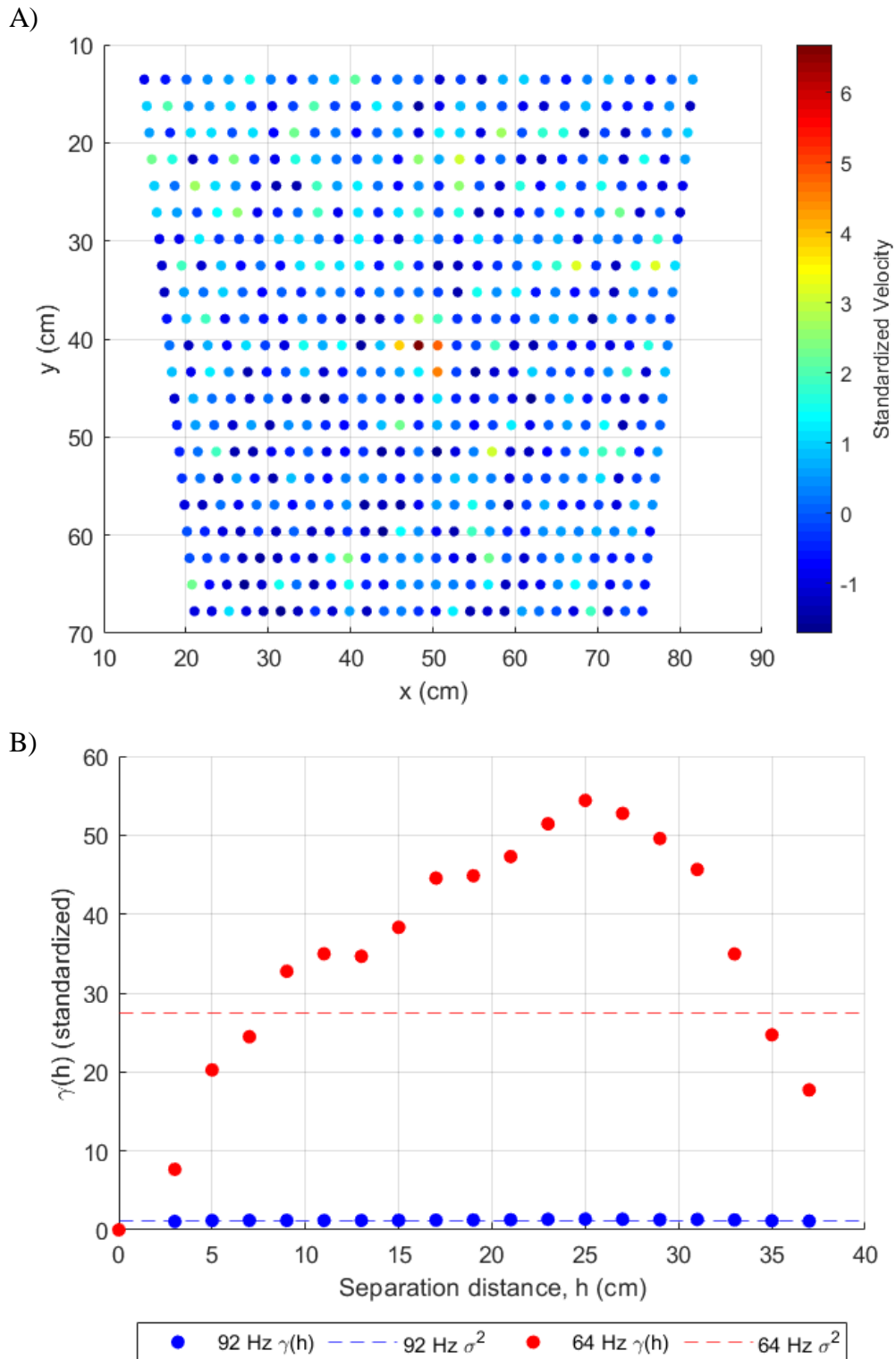
Figure 39. Velocity map and variogram of standardized and reduced velocity of target data at 92 Hz. A) Velocity map at 92 Hz; B) Variogram at 92 Hz and 64 Hz.
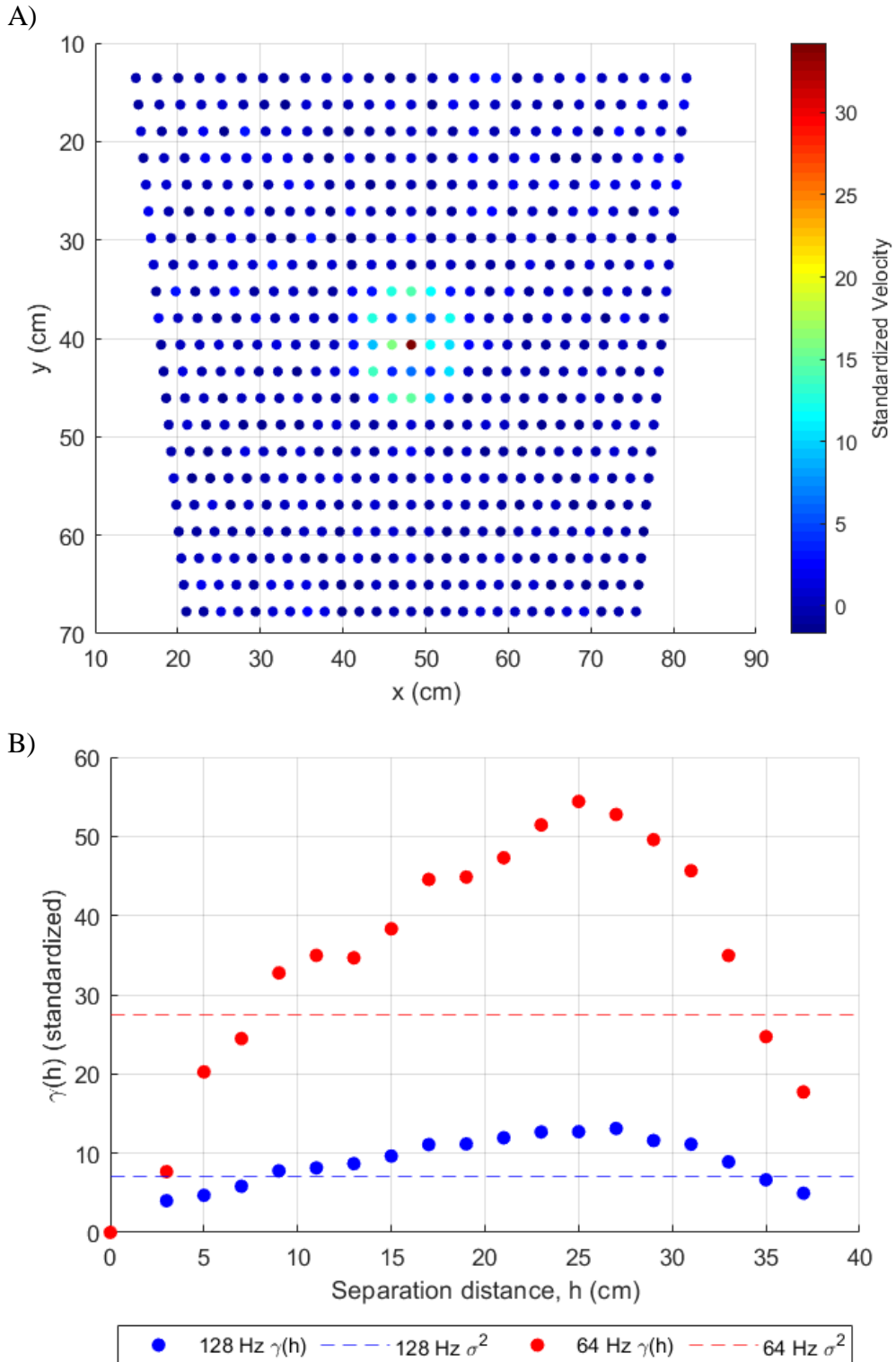
Figure 40. Velocity map and variogram of standardized and reduced velocity of target data at 128 Hz. A) Velocity map at 128 Hz; B) Variogram at 128 Hz and 64 Hz.

A)



B)
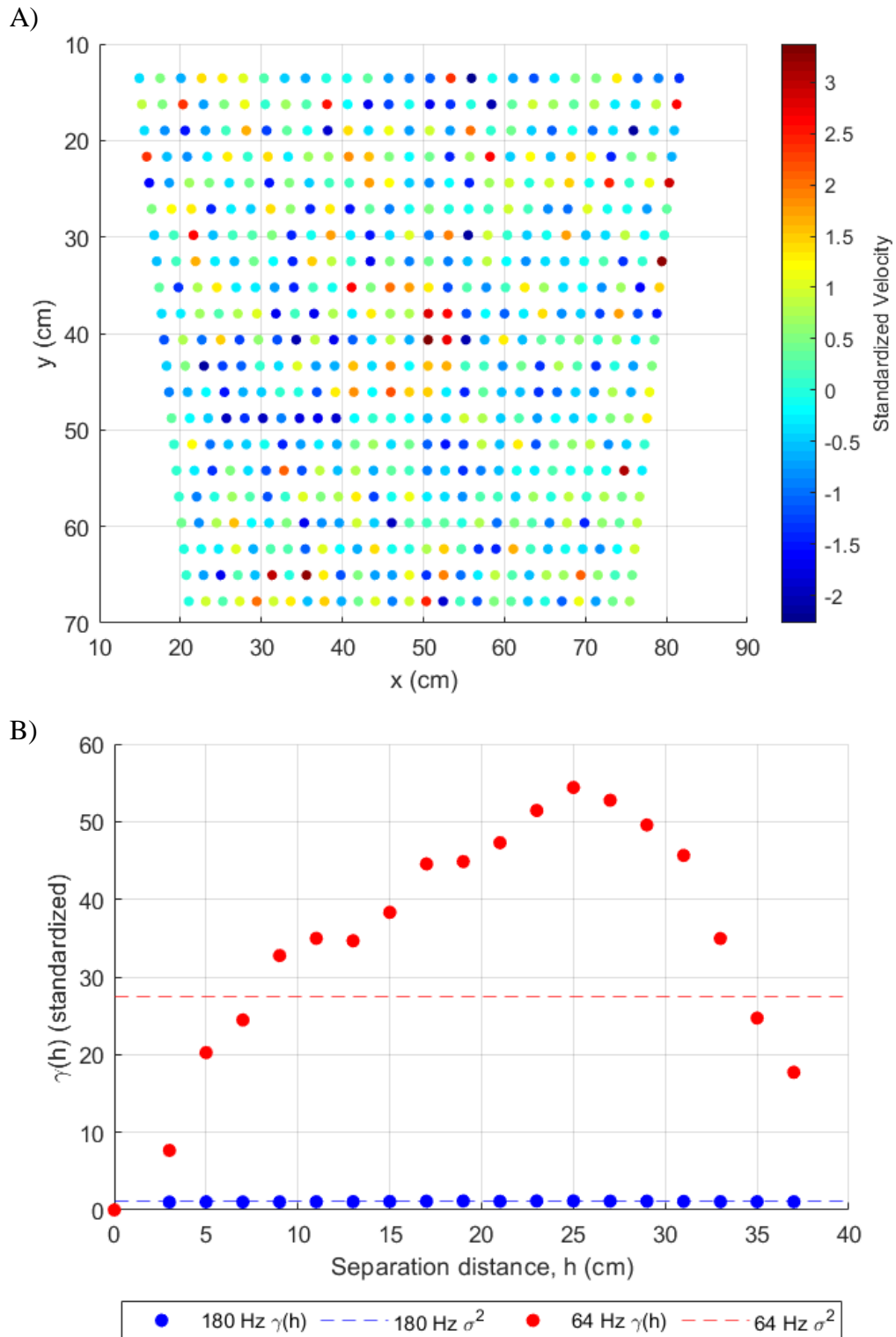


Figure 41. Velocity map and variogram of standardized and reduced velocity of target data at 180 Hz. A) Velocity map at 180 Hz; B) Variogram at 180 Hz and 64 Hz.

APPENDIX A

```matlab
%% Acquisition
%Anna McWhirter
%target present
clear
clc
close all
load('V.mat', 'V')
load('Vcmpx.mat', 'Vcmpx')

Vlm = [Vcmpx(:,1) V];

%reshape

A = abs(Vlm(:,2:end));

f = abs(Vlm(:,1));

B = zeros(31,37,91);

 for i = 1:length(f)

     B(:,:,i) = reshape(A(i,:),37,31)';

 end
a = 23;

F64 = ((B(:,:,a)));     %64 hz
F64v = F64(:);      %vector

Ab = abs(Vcmpx(:,2:end));

fb = abs(Vcmpx(:,1));

Bb = zeros(31,37,91);

 for i = 1:length(fb)

     Bb(:,:,i) = reshape(Ab(i,:),37,31)';

 end
```

```matlab
F64n = (Bb(:,:,a));      %64 hz
F64nv = F64n(:);       %vector

subplot(2,1,1)
plot(f,squeeze((B(24,25,:)))); %x33 y24 NOT on top of
target means row 24 column 33
hold on
xline(64,'r')
hold off
xlabel('Frequency (Hz)')
ylabel('Raw data velocity')
title('Row 24, Column33, off target')
ylim([0 2e-03])

subplot(2,1,2)
plot(f,squeeze((B(16,19,:))),'DisplayName','point
velocity'); %x19 y16 on top of target means row 16 column
19
hold on
xline(64,'r','DisplayName','64 Hz')
hold off
xlabel('Frequency (Hz)')
ylabel('Raw data velocity')
title('Row 16, Column 19, on target')
legend

%% coordinates
XL = 96.5;
dx = 12.7/30;
nc = 1:30;
xstart = 0+nc*dx;
xend = XL-nc*dx;
xinc = xend/37;

xtest = xstart(1,29):xinc(1,29):xend(1,29);

xr1 = 0:2.68:XL;
XL = 96.5;
dx = 0.423;
```

```matlab
nc = 1:30;
xstart = 0+nc*dx;
xend = XL-nc*dx;
xr = zeros(30,37);
for i = 1:length(nc)
    xr(i,:) = linspace(xstart(1,i),xend(1,i),37);
end

xreal = [xr1; xr];
X = xreal(:);

ystart = 0:2.71:81.3;
Y = repmat(ystart,1,37)';

yreal = zeros();
for i = 1:length(Y)
    yreal = reshape(Y,31,37);
end

%remove target
F64(15:17,17:21) = NaN;
F64(14,18:20) = NaN;
F64(18,18:20) =  NaN;
F64NaN = F64(:);
Fv = F64(:);

Fv(isnan(Fv))=[];

Tcount = numel(Fv);
Bcount = numel(F64nv);

%% remove outliers
%no target on target data:
[Bct,TFt,lowert,uppert,centert] =
filloutliers(Fv,'clip','median');
p = (1:Tcount);
figure;
plot(p,Fv,p,Bct,'o',p,uppert*ones(1,Tcount),p,centert*ones(
1,Tcount),p,lowert*ones(1,Tcount))
legend('Standardized Data','Filled Data','Upper
Threshold','Center','Lower Threshold')
```

```matlab
xlabel('Data points')
ylabel('Standardized velocity')
ylim([-.5e-04 3e-04])
xlim([0 1150])
grid on
% title('no target, target data')

%background data:
[Bc,TF,lower,upper,center] =
filloutliers(F64nv,'clip','median');
p = (1:Bcount);
figure;
plot(p,F64nv,p,Bc,'o',p,upper*ones(1,Bcount),p,center*ones(
1,Bcount),p,lower*ones(1,Bcount))
legend('Standardized Data','Filled Data','Upper
Threshold','Center','Lower Threshold')
xlabel('Data points')
ylabel('Standardized velocity')
grid on
xlim([0 1150])


%add target back in
ix = 511;
Bct = [Bct(1:ix-
1);F64v(511);F64v(512);F64v(513);Bct(ix:end)];
ix2 = 541;
Bct = [Bct(1:ix2-
1);F64v(541);F64v(542);F64v(543);F64v(544);F64v(545);Bct(ix
2:end)];
ix3 = 572;
Bct = [Bct(1:ix3-
1);F64v(572);F64v(573);F64v(574);F64v(575);F64v(576);Bct(ix
3:end)];
ix4 = 603;
Bct = [Bct(1:ix4-
1);F64v(603);F64v(604);F64v(605);F64v(606);F64v(607);Bct(ix
4:end)];
ix5 = 635;
Bct = [Bct(1:ix5-
1);F64v(635);F64v(636);F64v(637);Bct(ix5:end)];
```

```matlab
%% smaller grid
b = Bc;
t = Bct;

bm = reshape(b,31,37);       %stanB matrix, full grid
tm = reshape(t,31,37);       %stanT matrix, full grid

xnew = xreal(6:26,6:32);     %x matrix, small grid
xv = xnew(:);
ynew = yreal(6:26,6:32);     %y matrix, small grid
yv = ynew(:);
FB_small = bm(6:26,6:32);  %new stanB matrix, small grid
FBv = FB_small(:);           %new stanB vector, small grid

FT_small = tm(6:26,6:32);  %new stanT matrix, small grid
FTv = FT_small(:);           %new stanT vector, small grid

%% Standardize
%remove target
FTnotarget = FT_small;
FTnotarget(10:12,12:16) = NaN;
FTnotarget(13,13:15) = NaN;
FTnotarget(9,13:15) = NaN;
FTnotarget(isnan(FTnotarget)) = [];
FTntv = FTnotarget(:);  %Points surroudning the target

Bct_mean = mean(FTntv);
st_Bct = std(FTntv);

meanBoutrem = mean(FBv);
sb = std(FBv);

stanB = ((FBv)-abs(meanBoutrem))/(sb); %bkgr
stanT = ((FTv)-abs(Bct_mean))/(st_Bct);     %target

%%
c = F64v;
figure;
scatter3(X,Y,F64v,25,c(:),'filled')
axis ij
colormap(parula)
```

```matlab
colorbar
view(0,90)
xlabel('x (cm)')
ylabel('y (cm)')
grid on

cb = F64nv;
figure;
scatter3(X,Y,F64nv,25,cb(:),'filled')
axis ij
colormap(parula)
colorbar
view(0,90)
xlabel('x (cm)')
ylabel('y (cm)')
grid on

xgrid =
[xreal(6,6),xreal(26,6),xreal(26,32),xreal(6,32),xreal(6,6)
];
ygrid =
[yreal(6,6),yreal(26,6),yreal(26,32),yreal(6,32),yreal(6,6)
];
c = Bct;
figure;
scatter3(X,Y,Bct,25,c(:),'filled')
hold on
plot(xgrid,ygrid,'-k','LineWidth',3)
axis ij
colormap(parula)
colorbar
% caxis([-2 8])
view(0,90)
xlabel('x (cm)')
ylabel('y (cm)')
grid on


cb = Bc;
figure;
```

```matlab
scatter3(X,Y,Bc,25,cb(:),'filled')
hold on
plot(xgrid,ygrid,'-k','LineWidth',3)
axis ij
colormap(parula)
colorbar
view(0,90)
xlabel('x (cm)')
ylabel('y (cm)')
grid on

%Points surrounding the target location in the background
Bc_m = reshape(stanT,21,27);
Bctv = Bc_m;
Bctv(10:12,12:16) = NaN;
Bctv(13,13:15) = NaN;
Bctv(9,13:15) = NaN;
for i = 1:length(Bctv)
    Bctv(isnan(Bctv)) = [];
end
Bctv = Bctv(:);

Bc_matrix = reshape(stanB,21,27);
Bc_matrix(10:12,12:16) = NaN;
Bc_matrix(13,13:15) = NaN;
Bc_matrix(9,13:15) = NaN;
Bcv = Bc_matrix;
for i = 1:length(Bcv)
    Bcv(isnan(Bcv)) = [];
end
Bcv = Bcv(:);

%x edges small grid
xBct = xnew;
xBct(10:12,12:16) = NaN;
xBct(13,13:15) = NaN;
xBct(9,13:15) = NaN;
xBct = xBct(:);
for i = 1:length(xBct)
    xBct(isnan(xBct)) = [];
end
```

```matlab
xBct = xBct(:);

%y edges small grid
yBct = ynew;
yBct(10:12,12:16) = NaN;
yBct(13,13:15) = NaN;
yBct(9,13:15) = NaN;
yBct = yBct(:);
for i = 1:length(yBct)
    yBct(isnan(yBct)) = [];
end
yBct = yBct(:);

% ONLY target points
targetm = zeros(5,5);
targetm(1,2:4) = Bc_m(9,13:15);
targetm(2:4,1:5) = Bc_m(10:12,12:16);
targetm(5,2:4) = Bc_m(13,13:15);
targetv = targetm(:);

for i = 1:length(targetv)
    if targetv(i) == 0
        targetv(i) = NaN;
    end
end
targetv(isnan(targetv))=[];

%only target x coordinates
xtm = zeros(5,5);
xtm(1,2:4) = xreal(14,18:20);
xtm(2:4,1:5) = xreal(15:17,17:21);
xtm(5,2:4) = xreal(18,18:20);
xtv = xtm(:);

for i = 1:length(xtv)
    if xtv(i) == 0
        xtv(i) = NaN;
    end
end
xtv(isnan(xtv))=[];
```

```matlab
%only target y coordinates
ytm = zeros(5,5);
ytm(1,2:4) = yreal(14,18:20);
ytm(2:4,1:5) = yreal(15:17,17:21);
ytm(5,2:4) = yreal(18,18:20);
ytv = ytm(:);

for i = 1:length(ytv)
    if ytv(i) == 0
        ytv(i) = NaN;
    end
end
ytv(isnan(ytv))=[];

% just target
TargetMatrix = [xtv ytv targetv];
save('stanTarget.txt', 'TargetMatrix', '-ascii', '-double',
'-tabs')

%% change this to change plot display

b = stanB;
t = stanT;

meanB = mean(b);
meanT = mean(t);
uvT = meanT;
uvB = meanB;
count = numel(b);

X = xv;
Y = yv;
%% NUMBER OF PTS AND NEEDED ENCOUNTERS

J = count;       %number of points
j = 1:J;
k = 1:J;

%% ZERO SEPARATION INCLUDED PAIRS

syms k
```

```matlab
M = J+1-k;
symsum(M,k,1,count)


%% Matrix of separations btw sampled point

dd = zeros(count,count);
for k = 1:J
    for j = 1:J
        dd(k,j) = (sqrt((X(k)-X(j)).^2 + (Y(k)-Y(j)).^2));
    end
end

%dd_new = triu(dd);      %now same as MathCAD
[c,r] = meshgrid(1:size(dd,1),1:size(dd,2));
idx = c < r;
dd(idx) = NaN;
%% Matrix for cov (vdif) and variogram (vgam)

vdif = zeros(count,count);
for k = 1:J
    for j = 1:J
        vdif(k,j) = ((t(k)-uvT)*(t(j)-uvT));
    end
end
%diagonal is diff, everything else same
vdif = triu(vdif);


vgam = zeros(count,count);
for k = 1:J
    for j = 1:J
        vgam(k,j) = (t(k)-t(j)).^2;
    end
end
%everything the same as MathCAD

[c,r] = meshgrid(1:size(vgam,1),1:size(vgam,2));
idx = c < r;
vgam(idx) = NaN;
vdif(idx) = NaN ;
```

```matlab
%% reorder matrices

dd_new = reshape(dd',[],1) ;
dd_new(isnan(dd_new)) = [] ;       %separations

vdif_new = reshape(vdif',[],1) ;
vdif_new(isnan(vdif_new)) = [] ;      %covariance

vgam_new = reshape(vgam',[],1) ;
vgam_new(isnan(vgam_new)) = [] ;      %variance

%% combine into matrix

rDat = [dd_new,vdif_new];
sDat = sortrows(rDat,1);

rgDat = [dd_new,vgam_new];
sgDat = sortrows(rgDat,1);

% V_test = sum((F64v-uv).^2)/(length(F64v)-1);
%% COVARIANCE

nlags = 20;
range = 40;
n = 1:(nlags-1) ;
E(n+1) = (range/nlags)*n;
E(1) = 0.1;
E(2) = 2;
VarT = var(t);

V1 = zeros(nlags-1,1) ;
V2 = V1 ;

for n = 1:(nlags-1)
   I = 0 ;
   I = I + sum((E(n)<=sDat(:,1)) & (sDat(:,1) < E(n+1))) ;
   U = sum(sDat((E(n)<=sDat(:,1)) & (sDat(:,1) <
E(n+1)),2)) ;

   V1(n) = U/I ;
   V2(n) = I ;
End
```

```matlab
EE = E(2:end) - (E(2:end)-E(1:end-1))/2 ;

figure;
hold on
p(1) = 
scatter(EE,V1,'b','filled','DisplayName','Covariance');
p(2) = yline(VarT,'--r','DisplayName','Variance');
p(3) = scatter(0,VarT,'b','filled');
hold off
xlabel('Separation distance, h (cm)')
ylabel('C(h) (standardized data)')
legend(p([1 2]),'Location','southeast')
grid on
ylim([-5 30])

figure;
scatter(EE,V2,'b','filled')
ylabel('Number of Pairs')
xlabel('Separation distance, h (cm)')
grid on


%% VARIOGRAM

V1v = zeros(nlags-1,1) ;
V2v = V1v ;

for n = 1:(nlags-1)
    II = 0 ;
    II = II + sum((E(n)<=sgDat(:,1)) & (sgDat(:,1) <
E(n+1))) ;
    UU = sum(sgDat((E(n)<=sgDat(:,1)) & (sgDat(:,1) <
E(n+1)),2)) ;

    V1v(n) = UU/II ;
    V2v(n) = II ;

end

EE = E(2:end) - (E(2:end)-E(1:end-1))/2 ;

Vv = (V1v./2)';
```

```matlab
figure;
hold on
p(1) = scatter(EE,Vv,'b','filled','DisplayName','Variogram
Value');
p(2) = yline(VarT,'--r','DisplayName','Variance');
p(3) = scatter(0,0,'b','filled');
hold off
xlabel('Separation distance, h (cm)')
ylabel('\gamma(h) (standardized data)')
legend(p([1 2]),'Location','southeast')
grid on
ylim([0 60])

%% BACKGROUND
% Matrix of separations btw sampled point
dd = zeros(count,count);
for k = 1:J
    for j = 1:J
        dd(k,j) = (sqrt((X(k)-X(j)).^2 + (Y(k)-Y(j)).^2));
    end
end

%dd_new = triu(dd);
[c,r] = meshgrid(1:size(dd,1),1:size(dd,2));
idx = c < r;
dd(idx) = NaN;

% Matrix for cov (vdif) and variogram (vgam)
vdif = zeros(count,count);
for k = 1:J
    for j = 1:J
        vdif(k,j) = ((b(k)-uvB)*(b(j)-uvB));
    end
end
vdif = triu(vdif);

vgam = zeros(count,count);
for k = 1:J
    for j = 1:J
        vgam(k,j) = (b(k)-b(j)).^2;
    end
end
```

```matlab
%everything the same as MathCAD
[c,r] = meshgrid(1:size(vgam,1),1:size(vgam,2));
idx = c < r;
vgam(idx) = NaN;
vdif(idx) = NaN ;

%% reorder matrices
dd_new = reshape(dd',[],1) ;
dd_new(isnan(dd_new)) = [] ;

vdif_new = reshape(vdif',[],1) ;
vdif_new(isnan(vdif_new)) = [] ;

vgam_new = reshape(vgam',[],1) ;
vgam_new(isnan(vgam_new)) = [] ;
%% combine into matrix
rDat = [dd_new,vdif_new];
sDat = sortrows(rDat,1);
rgDat = [dd_new,vgam_new];
sgDat = sortrows(rgDat,1);
%% COVARIANCE
nlags = 20;
range = 40;
n = 1:(nlags-1) ;
E(n+1) = (range/nlags)*n;
E(1) = 0.1;
E(2) = 2;
VarB = var(b);
V1 = zeros(nlags-1,1) ;
V2 = V1 ;
for n = 1:(nlags-1)
    I = 0 ;
    I = I + sum((E(n)<=sDat(:,1)) & (sDat(:,1) < E(n+1))) ;
    U = sum(sDat((E(n)<=sDat(:,1)) & (sDat(:,1) <
E(n+1)),2)) ;

    V1(n) = U/I ;
    V2(n) = I ;

end
```

```matlab
EE = E(2:end) - (E(2:end)-E(1:end-1))/2 ;


figure;
hold on
p(1) =
scatter(EE,V1,'b','filled','DisplayName','Covariance');
p(2) = yline(VarB,'--r','DisplayName','Variance');
p(3) = scatter(0,VarB,'b','filled');
hold off
xlabel('Separation distance, h (cm)')
ylabel('C(h) (standardized data)')
legend(p([1 2]),'Location','east')
grid on
ylim([-5 30])
% scatter(0,VarB,'filled')

figure;
scatter(EE,V2,'b','filled')
ylabel('Number of Pairs')
xlabel('Separation distance, h (cm)')
grid on

%% VARIOGRAM
V1v = zeros(nlags-1,1) ;
V2v = V1v ;

for n = 1:(nlags-1)
    II = 0 ;
    II = II + sum((E(n)<=sgDat(:,1)) & (sgDat(:,1) <
E(n+1))) ;
    UU = sum(sgDat((E(n)<=sgDat(:,1)) & (sgDat(:,1) <
E(n+1)),2)) ;

    V1v(n) = UU/II ;
    V2v(n) = II ;

end

EE = E(2:end) - (E(2:end)-E(1:end-1))/2 ;
Vv = V1v./2;
```

```matlab
figure;
hold on
p(1) = scatter(EE,Vv,'b','filled','DisplayName','Variogram
Value');
p(2) = yline(VarB,'--r','DisplayName','Variance');
p(3) = scatter(0,0,'b','filled');
hold off
xlabel('Separation distance, h (cm)')
ylabel('\gamma(h) (standardized data)')
legend(p([1 2]),'Location','east')
grid on
ylim([0 60])
```

APPENDIX B

```
1                                                          !Number of fields

32 32.                                                     !MAXBLK,L

24246                                                      !Field lnk - Random Number Seed

0.0  1                                                     !Field lnk - Mean and variance

2  10  10                                                  !Field lnk - cov type, scalex,scaley
```

Appendix B.1. Input file containing information to be used in calculation of the random field
with fixed correlation lengths. The output is a file with three columns, with x- and y- coordinates
and the associated value. The data was clipped from a 32 by 32 grid output to fit the dimensions
of observations.

VITA

Anna Marie McWhirter was born and raised in Arlington, Texas. She graduated from Lamar High School and went on to earn her Bachelor of Science in Geological Engineering from the University of Mississippi (Ole Miss or UM). In undergrad, she was an active member of Phi Mu – Alpha Delta Chapter (2013-2017), Society for Women Engineers (2016-2020), and the Honor Society of Phi Kappa Phi (2019-2020). In 2017 and 2018, Anna Marie was a student representative for the University of Mississippi Engineering Advisory Board and served as a Teaching Assistant for Elsie Okoye in Engineering Analysis and Environmental Geology. She was the President of the American Association of Petroleum Engineers (UM Chapter 2017-2018) and the Association of Engineering and Environmental Engineers (UM Chapter 2017-2018). She was also the Vice President for Sigma Gamma Epsilon (UM Chapter 2017-2018). Her love for physical processes and the geological industry led her to continue education at the university. She worked under Dr. Robert Holt as a Research Assistant with the National Center for Physical Acoustics on an Office of Naval Research project proposal, led by Dr. Craig Hickey.

Although commencement is postponed, Anna Marie will be graduating from the University of Mississippi earning a Master of Science in Engineering Science with an Emphasis in Hydrology (May 2020). She secured a dream engineering job with TTL, Inc. in the Environmental Engineering Industry.